The Development of a Cartilage Specific Bioink for Three-Dimensional Bioprinting

Esther Kingma

Thesis Report

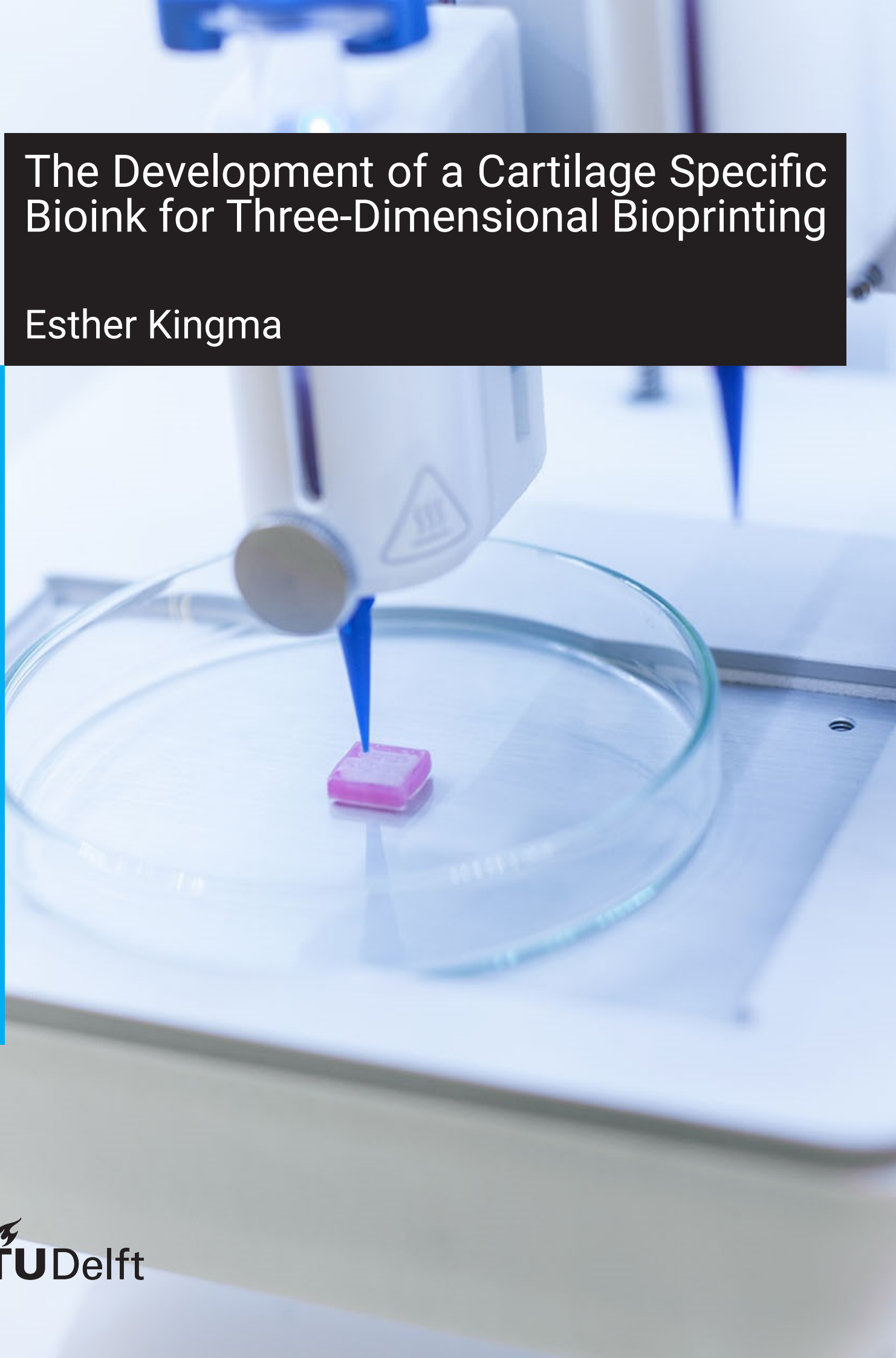

TU Delft

The Development of a Cartilage Specific Bioink for Three-Dimensional Bioprinting

by

Esther Kingma

to obtain the degree of Master of Science
at the Delft University of Technology,
to be defended publicly on July 28, 2021 at 09:30 AM.

Student number:	4393309	
Master program:	MSc. Biomedical Engineering	
Master track:	Musculoskeletal Biomechanics	
Thesis committee:	Prof. Dr. A. A. (Amir) Zadpoor,	TU Delft
	Dr. Ir. E. L. (Lidy) Fratila-Apachitei,	TU Delft
	Dr. E. C. M. (Elizabeth) Carroll,	TU Delft
	Dr. P. J. (Pedro) Díaz Payno,	TU Delft, supervisor

TU Delft

Acknowledgements

I wish to express my sincere appreciation to my daily supervisor, Postdoc Pedro Diaz Payno, who monitored my project every step of the way. He showed me how to perform all the biochemical and histological procedures and taught me the basic principles of cell culture. I really enjoyed the time we spent in the lab together. We worked long lab days, particularly while bioprinting with cells, sometimes with stress but we still had a good time together. I could always reach out to him for advice, and without his persistent help, the goal of this project would not have been realized. I also would like to express my gratitude to my supervisor, Assistant professor Dr. Ir. E. Lidy Fratila-Apachitei, who monitored my progress and was there when I needed her. Every two weeks, I looked forward to our bioprinting cluster meetings. Even though finishing the presentations on time was sometimes challenging, I really appreciated the opportunity to present and to get feedback. I am also grateful to Professor Dr. Ir. Amir Zadpoor, who attended the cluster meetings and always provided me with helpful criticism and recommendations. I would like to give a special thanks to Maria Kalogeropoulou. We met in the beginning of our graduate projects and quickly became close friends. We often discussed our thesis progress, gave feedback on one other's work, battled our way through long lab hours together, and celebrated small lab successes with drinks and coffee. I am really glad I met her and this thesis would not have been the same without her. Also, I wish to thank my friend/housemate Daphne Nesenberend, who has also been there every step of the way. Together, we worked on our reports, motivated each other to go on, and took needed breaks with Gilmore Girls. Finally, I wish to thank my family and all my close friends. They kept me going and this work would not have been possible without their support.

Esther Kingma
Delft, July 2021

Abstract

Bioprinting is a promising technique that has the ability to generate complex tissue structures for articular cartilage (AC) repair and regeneration. However, most biomaterials used for bioprinting are incapable of representing the complexity of native extracellular matrix (ECM). In this study, a novel cartilage specific bioink has been developed with tyramine modified hyaluronic acid (THA) and decellularized ECM (dECM) of AC for three-dimensional bioprinting, combining the printable qualities of THA with AC dECM to create an optimized microenvironment. First, the influence of increasing concentrations of AC dECM on the rheological and printability properties was assessed. Next, human mesenchymal stem cells (hMSCs) were incorporated into bioinks composed of 2.5% w/v THA and AC dECM (0.0%-1.0% w/v). The THA-AC dECM bioinks have been successfully bioprinted into stable scaffolds with viable cells and were cultured for 28 days in chondrogenic differentiation medium. Subsequently, the effect of combining AC dECM with THA was evaluated by measuring the cell viability, cell differentiation and AC tissue deposition. The ink compositions with AC dECM (0.5% and 1.0% w/v) caused an increase in ink viscosity, yield stress and damping factor compared to the THA ink, but still showed shear thinning behavior and provided good printability. Spread cell morphology was observed for the scaffolds with addition of AC dECM compared to AC dECM free control with only THA, indicating enhanced cell adhesion to the hydrogel network. Moreover, a higher production of sulfated glycosaminoglycans (sGAGs) was observed for the scaffolds where AC dECM was added. The THA and AC dECM bioink composition showed promising results for AC tissue engineering and warrants further research into the development of bioinks with tissue-specific inductive properties.

Contents

1 Introduction

When articular cartilage (AC) is damaged by trauma or disease, recovery can be difficult, eventually leading to impairment of joint function and structure [1]. Articular cartilage is a load-bearing tissue that covers the ends of the bones and allows friction-free movement. Overall, cartilage tissue consists of collagen, glycosaminoglycans (GAGs), water and a limited number of cells. The combination of the low number of cells and the lack of nerves and vasculature, limits the regenerative capacity of the tissue [2]. As a result, untreated articular cartilage defects can lead to diseases, resulting in disability and a reduction in quality of life [3, 4].

Over the years, different treatment methods have been proposed to recover from AC damage, though they still have limited effect. Procedures such as pain killers or the use of anti-inflammatory drugs may alleviate the symptoms, but do not treat the cause of the disease and only delay the onset [5]. Promising approaches are surgical interventions aiming to regenerate the tissue, such as autologous chondrocyte implantation, microfracture and osteochondral grafting. Despite their clinical use, these techniques have mixed results, since they do not fully restore the function of healthy cartilage [4, 6]. Moreover, these approaches show other shortcomings: invasive surgery, donor site morbidity, time-consuming, high costs and difficulty in achieving an implant with a similar shape as the injury site [4, 5].

For these reasons, the tissue engineering field has been motivated to treat AC defects. In order to treat such defects, new bio-engineering technologies such as three-dimensional (3D) bioprinting have been developed [7]. Bioprinting allows precise deposition of cell-laden hydrogels in an anatomically relevant and patient-specific design [7]. The success of bioprinting is highly dependent on the composition of bioink, defined as a combination of cells, biomaterials and bioactive cues suitable for automated biofabrication technologies [8]. In order to be printed, bioinks must also meet the appropriate design specifications. For bioprinting, a bioink should have suitable mechanical and biological properties to ensure shape fidelity without compromising cell viability [9]. A bioink should be viscous and show shear thinning behavior so it is able to flow through a nozzle. However, bioink should not be too viscous, since increasing shear forces exerted on the cell-laden bioink could decrease cell viability [10]. Or, when a bioink is not viscous enough, it will flow quickly after deposition, decreasing the shape fidelity of the printed filaments [6]. Furthermore, a bioink

should be able to retain its shape after printing and have sufficient mechanical integrity to support additional deposited ink without collapsing [11]. Moreover, a bioink should provide a suitable environment for cells to survive and to promote cell proliferation, migration and differentiation [9].

Currently, bioinks are developed with unmodified and modified biopolymers, such as alginate, fibrin, hyaluronic acid (HA), gelatin and decellurized extracellular matrix (dECM). Hyaluronic acid is an promising material for AC regeneration, given that it is one of the main components of the extracellular matrix (ECM) of AC. In native tissue, HA interacts with the cell surface receptor, CD44, and has the osmotic capacity to hold large amounts of water, providing compressive strength through fluid retention [12, 13]. However, native HA solutions are not suitable for bioprinting, due to flow upon deposition.

Therefore, native HA is often combined with other polymers to guarantee stability after printing. Or shape retention is achieved by modifying HA, so crosslinking strategies can be implemented. A few studies have reported bioprinting of modified HA as a one component bioink with good printability. The most common bioink formulation is methacrylate HA (MeHA), which is photo-crosslinked using UV-light and Irgacure 2959 as a photoinitiator [14]. Another printable formulation was obtained by modifying HA with adamantane and β-cyclodextrin (Ad,-MeHA/CD-MeHA) for a self healing guest-hosted based bioink [15, 16]. The two components formed a guest-host assembly upon mixing and UV-light photo-crosslinking was employed to ensure structural stability. Recently, Petta et al. developed a single-component, tyramine-modified HA (THA) bioink with good shape fidelity and stability, using two distinct crosslinking mechanisms [17, 18]. Although some of these bioinks were successfully bioprinted into cell-printed structures and HA has the ability to interact with cells using surface receptor CD44, minimal cell-biomaterial interactions were observed [15, 17]. Moreover, it has been observed that HA hydrogels, used for cell growth and tissue remodeling, show poor cell attachment [18, 19].

In addition to the limitations mentioned above, bioprinting studies have failed to engineer hyaline articular cartilage that mimics human tissue. Partially, this can be explained by the lack of a suitable microenvironent that favours cartilage matrix production. In recent years, there has been increased interest in the use of tissue-specific matrix to improve tissue engineered structures [20]. The ECM is composed of tissue specific cytokines, macromolecules and growth factors, providing cellular cues that regulate cell behavior [21]. When the ECM is decellurized, it preserves parts of the ECM components and could therefore provide both structural and functional cues to cells [20, 22]. dECM has already been used to fabricate molded scaffolds and has shown promising results for AC regeneration due to their chondro-inductivity [22–25]. Furthermore, Kesti et al. used AC dECM for bioprinting, where dECM was incorporated into an alginate/gellan hydrogel [26]. The addition of dECM to the bioink stimulated more chondrocyte prolifiration compared to the hydrogel alone. In comparison, Chen et al. developed a bioink by combining dECM with HA, gelatin, and PLGA [27].

The objective of this thesis is to develop a novel cartilage specific bioink for 3D bioprinting with THA and AC dECM. This bioink combines the printable qualities of THA with

AC dECM to create an appropriate microenvironment that regulates cell behavior. Two crosslinking methods are involved in the polymerization of THA, enzymatic pre-crosslinking mediated by horseradish peroxidase (HRP) and hydrogen peroxide (H_2O_2) to control the extrusion properties, and photo-crosslinking triggered by visible light and Eosin Y (EO) for shape fixation of the printed scaffold. For the dECM of AC, almost all the sGAG were removed during the solubilization process and the dECM mostly consist of collagen. The first a printable ink composition for THA was obtained with rheology and printability measurements. Subsequently, the impact of various concentrations of dECM AC in the THA ink on printability was examined. Next, the photo-crosslinking process was optimized to obtain scaffolds with high resolution and shape fidelity. After optimization of the bioink and scaffold properties, the influence of the bioink composition on cell viability was assessed. Finally, we bioprinted THA and AC dECM bioinks embedded with human mesenchymal stem cells (hMSCs). The effect of combining AC dECM with THA was evaluated by measuring the cell viability, cell differentiation, and tissue deposition of the cell-laden scaffolds.

2

Materials and Methods

2.1. Materials and Reagents

Tyramine-modified hyaluronic acid (THA) sodium salt from *Streptococcus equi* with an average molecular weight of 280 kDa was kindly provided to us by the AO Research Institute Davos (Davos Platz, Switzerland) [17, 18]. The degree of substitution (DS), defined as the percentage of HA carboxyl groups functionalized by tyramine, has a final value of 6%. Solubilized articular cartilage ECM was also kindly provided to us by Professor Daniel J. Kelly (Trinity College Dublin, Ireland) [22, 28]. All the reagents used in this study, Horseradish peroxidase (HRP), Hydrogen peroxide (H_2O_2), Eosin Y (EO), Phosphate buffered saline (PBS), Calcein-AM (Ca-AM), Ethidium Homodi- mer-1 (EthD-1), Presto Blue, paraformaldehyde (PFA), Alcian Blue, Nuclear Fast Red, HARRIS Hematoxylin and Direct Red 80 were purchased from Sigma-Aldrich. αMinimum Essential Medium (αMEM) and Dulbecco's Modified Eagle Medium (DMEM, high glucose, GlutaMAX^{TM} supplement and HEPES) were purchased from Gibco, ThermoFisher.

Table 2.1: Overview of the concentrations THA and AC dECM for the three evaluated bioink formulations with abbreviations.

	Polymer concentration (% w/v)	
Abbreviation	THA	AC dECM
$THA_{2.5}$	2.5	0.0
$THA_{2.5}$-$AC_{0.5}$	2.5	0.5
$THA_{2.5}$-AC_1	2.5	1.0

2.2. Bioink

For this study three different inks were prepared, containing a fixed concentration of THA (2.5% w/v) and a varying concentration of AC dECM (0.0%, 0.5%,1.0%). The abbreviations used for these inks and hereafter used in this report are shown in Table 2.1. To prepare the inks, THA and AC dECM were rehydrated with 1x PBS and 0.1 U/ml HRP. To dissolve THA and AC dECM, the inks were first mixed between two syringes (luor lock connection) and thereafter the inks were kept overnight under rotation (4 rpm) at 4°C covered in aluminum foil to protect the samples from light. After complete dissolution of THA and AC dECM, enzymatic crosslinking was triggered by adding H_2O_2. In addition EO and PBS were added, to

reach the desired final composition. To remove any air bubbles, the inks were centrifuged for 5' at 200g. Next, the inks were covered in aluminium foil, due to light sensitivity of the THA, and left for 60' at room temperature to crosslink. After enzymatic crosslinking, the network of the ink was broken down a bit by passing the ink through a nozzle three times, using a 25G nozzle and syringe. Causing the ink to be more homogeneous, which helps to keep the printing parameters constant. The final concentrations used in the inks are 2.5% w/v THA, 0.0%-1.0% w/v AC dECM, 0.1 U/ml HRP, 0.01% w/v EO and 0.1-0.3 mM H_2O_2, presented in Table 2.2.

Table 2.2: Volumes for preparation of THA and AC dECM bioinks with and without cell encapsulation.

Stock solutions	**Volumes to prepare for 1ml of THA-AC gel**			**Final concentrations**
	Cell free + no light crosslinking	**Cell free + light crosslinking**	**Cell loaded + light crosslinking**	
THA DS 6%	25 mg	25 mg	25 mg	2.5 % w/v
AC dECM	0, 5 or 10 mg	0, 5 or 10 mg	0, 5 or 10 mg	0, 5 or 10% w/v
Culture medium or PBS	600 µl	600 µl	600 µl	60% v/v
HRP 1 U/ml	10 µl	10 µl	10 µl	0.1 U/ml
EO 1.0% w/v	-	20 µl	20 µl	0.01% w/v
Cells suspended in medium	-	-	100 µl	
H_2O_2 1 mM	100, 250 or 300 µl	250 µl	300 µl	0.1, 0.25 or 0.3 mM
Culture medium or PBS	Fill up with PBS to achieve final volume of 1000 µl	Fill op with PBS to achieve final volume of 1000 µl	Fill op with medium to achieve final volume of 1000 µl	10, 15 or 30% v/v

2.3. Rheology characterization of the bioinks

The rheological characterization of the various inks is performed with a stress-controlled rheometer (Physica MCR 501; Anton Paar, Graz, Austria). The rheometer was equipped with a steel cone and plate geometry (diameter 30 mm, cone 1°). The temperature of the rheometer was controlled by a hood covering the whole cone/plate system and a Peltier plate connected to the lower plate. For all measurements the rheometer was preheated to 21°C.

Four ink properties were measured with the rheometer: the damping factor, the viscosity, the yield stress and the recovery modulus (measurements were repeated three times, n = 3). The inks for rheological measurements are prepared as explained in Section 2.2, without the EO needed for photo-crosslinking. Each rheological measurement start with a time dependence for 5 minutes to distribute the sample evenly between the plates, using a small-amplitude oscillatory shear at a frequency of 0.5 Hz and strain amplitude of 0.5%. The viscoelastic range was determined by a frequency sweep ranging between 0.1-10 Hz at a constant strain amplitude of 1.0%. The damping factor ($\tan\delta$ = G"/G') was calculated from the ratio of the storage modulus (G') and loss modulus (G") values at 1 Hz. The damping factor can be used to predict the successful extrudability and printability of an ink [17, 18]. Extrusion was experimentally validated by passing the ink through a 25G conical nozzle, while printability was validated by examining the retention of the shape-fidelity ratio of the extruded filaments The formulation were described as 'poor printability' when the extruded inks were to fluid to retain its shape, or when the printed filament was granular/ uneven. The formulations were defined as 'good printability' when the printed fila-

ments kept their designed shape.

The viscosity curves were determined by applying a shear stress ramp from of 0.1 to 10000 Pa with 20 points per decade. For the yield stress, defined as the shear stress at the crossover point of the storage (G') and loss (G") moduli, was determined by applying an oscillatory stress sweep with 50 logarithmic spaced shear stresses between 1-5000 Pa at a frequency of 0.5 Hz. The material recovery was obtained by subjecting the samples to a shear stress above the yield stress, mimicking the extrusion and flow through a nozzle, and measuring the G' before and after the stress test. The initial storage modulus (G'_{In}) was calculated by the averaging the G' of the initial 5' of the ink being exposed to oscillatory shear at a frequency of 0.5 Hz and strain amplitude of 0.5%. During the oscillatory stress sweep the sample was exposed to stresses higher than the material's yield stress. Thereafter, the recovery of the samples was measured for 10' in the third step of the protocol. The recovered storage modulus (G'_{Recov}) was determined by measuring the G' 1 minute after the oscillatory stress sweep was finished. The percentage of recovery was determined by dividing G'_{Recov} by G'_{In} and multiplying by 100%. An schematic overview of the four properties are shown in Fig. 2.1.

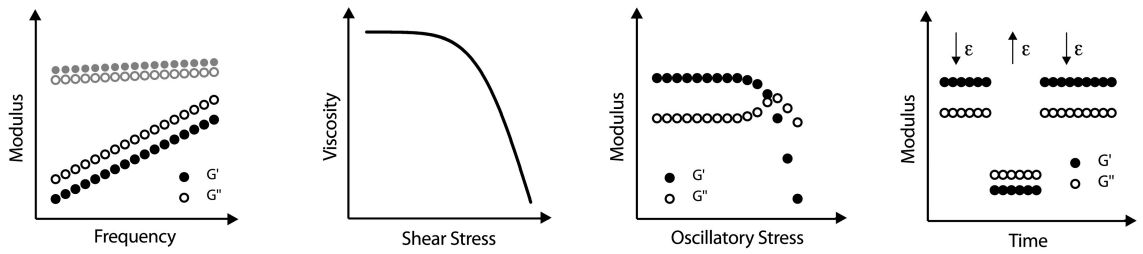

Figure 2.1: Overview of rheological tests needed to calculate ink properties: damping frequency sweep (damping factor), stress ramp (viscosity), oscillatory stress ramp (yield stress) and measuring G and G" before and after stress test (recovery modulus).

2.4. Photo-crosslinking of the scaffolds

To test the influence of photo-crosslinking on shape retention, scaffolds were printed with a $THA_{2.5}$ ink. The ink was prepared as explained in Section 2.2 with EO for photo-crosslinking. The printing was carried out with a Bio X bioprinter (Cellink). A square scaffold, 5 mm x 5 mm x 2.4 mm (L x W x H) was designed using Solidworks student software and converted to a G-Code file with Ultimaker Cura 4.7. The structure was printed on a glass microscope slide (76 mm x 26 mm, Thermo Scientific). Following printing, the scaffolds were crosslinked with green light (λ=522 and intensity 10W) for 5' or 10' from the top side or both sides (top and bottom scaffold). Images of the printed scaffolds were captured with the Wi-Fi Digital Microscope (ROTEK, resolution of 1280 x 720 pixels) directly after crosslinking. ImageJ was used to measure the length and width of printed structures.

2.5. Cell culture

This study used human mesenchymal stem cells isolated from bone marrow (hMSCs, Lonza). The hMSCs were frozen in cryovials of 1 ml, containing over 750.000 cells with more then

70% viability at passage 2. To initiate the cell culture process, cryovials were thawed for 1.5' in a 37°C waterbath. Next, the thawed cells were gently mixed with 20 ml of αMinimum Essential Medium (αMEM, Thermo Fisher), containing the following growth supplements: 1:10 fetal boving serum (FBS), 1:1000 Gentamycine, 1:167 Fungizone, 1:1700 Absorbic Acid (AA) and 1:5000 basic fibroblast growth factor (FGF) (CloneticsTM CGMTM BulletKitTM, Lonza). After mixing, the cells were centrifuged at 200g for 5' at room temperature to create a pellet. The supernatent was removed, to remove the freezing medium containing DMSO, and the cells were gently resuspended in fresh medium. To seed the cells, 500.000 cells and 20 ml of expansion medium were added per flask (T175, ThermoFisher). The cells were cultured in a incubator at 37°C, 5% $CO2_2$ and 90% humidity. To expand the cells, the flasks were refreshed two times a week with 20 ml expansion medium per flask.

Once the cells reached 90% confluency, the cells were passaged. This process was initiated by removing medium from the flasks. Subsequently, the cells were washed twice with 5 ml of HEPES-Buffered Saline Solution (HEPES-BSS, MSCs ReagentPackTM, Lonza). To detach the cells from the flasks, the cells were covered with trypsin (MSCs ReagentPackTM, Lonza) for 5' to 10' at 37°C. After the cells were released, 10 mL Trypsin Neutralizing Solution (TNS, MSCs ReagentPackTM, Lonza) was added per flask and the cell mixture was added to a 50 ml tube. The cells were then centrifuged into a pellet for 5' at 200g and the supernatant containing the trypsin/TNS solution was discarded. The pellet was resuspended in 2 ml of expansion medium. Next, the total number of cells was counted by using the Trypan Blue method. For the cell counting, 20 µl of cell suspension and 20 ml Trypan Blue were mixed in a 500 µl tube. In duplicate, 10 µl of the mixture was pipetted into a counting slide and thereafter the slide was inserted into a TC20 cell counter (Biorad) to count the cells. The cell counter automatically counts the total amount of cells/ml present, the amount of live cells/ml and the cell viability percentage. The cells were reseeded into a new flasks with a concentration of 500.000 cells per flask at a density of 2857 cells/cm2 to further expand them as described above until passage 3 or 4, before using them for the bioprinting experiments.

2.6. Pellet study

In order to perform the pellet study, flask containing hMSCs (expanded to passage 3) were washed with HEPES buffer, trypsinized and counted as described in 2.5. After cell counting, cells were divided over 1.5 ml autoclaved Eppendorf tubes to create pellets. For this study, the tubes were pierced with a needle to create a small hole, allowing the diffusion of oxygen inside the tube. To form the pellets, the tubes were centrifuged for 10' at 200g. The supernatent was removed and 500 µl of chondrogenic medium was added to the pellets, containing Dulbecco's Modified Eagle Medium (DMEM, ThermoFisher), 1:167 Fungizone, 1:1000 Gentamycine, 1:100 Sodium pyruvate, 1:100 Insulin Transferring Selenic acid (ITS+), 1:500 L-Proline, 1:1700 AA, 1:10000 Dexamethasone (Dex) and 1:200 Transforming growth factor beta 1 (TGF-β1). The pellets were cultured at 37°C, 5% $CO2_2$ and 90% humidity incubator and the medium was refreshed 2 times a week. In total 3 pellets, cultured till day 28, were used for this study. On day 21, the pellets were fixed using 4% w/v paraformaldehyde (PFA) overnight at 4°C. After fixation, pellets were transferred to PBS before performing further histological analysis.

2.7. Cell viability analysis before bioprinting

To test the influence of materials on the cells before bioprinting them, a preliminary study using a syringe without nozzle was performed. For this study two bioinks were prepared: $THA_{2.5}$ and $THA_{2.5}$-AC_1. To prepare the bioinks it was essential to sterilize all the materials, avoiding the risk of contamination. Therefore, the solutions (HRP, expansion medium, EO and H_2O_2) were sterilized with a 0.2 µm filter and the powders (THA and AC dECM) were exposed to UV light of the biosafety cabinet for 15'. Subsequently, the bioinks were prepared as described in Section 2.2 with the following composition: 2.5% w/v THA, with and without 1.0% w/v AC dECM, 0.1 U/mL HRP, 0.01% EO, 0.3 mM H_2O_2 and expansion medium to reach the desired final composition. Once the bioinks were crosslinked, hMSCs at passage 4, prepared and counted as described in Section 2.5, were suspended in expansion medium and mixed with bioinks to a final concentration of 3 x 10^6 cells/mL. The cells were embedded in the ink by using two syringes (connected by luer lock adapter), gently mixing the solution back and forth until it became a homogeneous mixture. To create the samples, bioink drops (average volume of 56 µl per sample) were formed by carefully pushing some bioink from the syringe opening on a glass slide. When all the drops were produced, the bioink was further crosslinked using green light (λ=522 and intensity 10W). Photoexposure was performed for 10' in total, 5' from the top and 5' from the bottom, to obtain a homogeneously crosslinked construct. Immediately after crosslinking the samples were transferred to a 48 well plate together with expansion medium. The medium was changed two times a week, using 1 ml of expansion medium for every well. In total 6 samples were formed and used for L/D analysis (n=3, day 2 and 8).

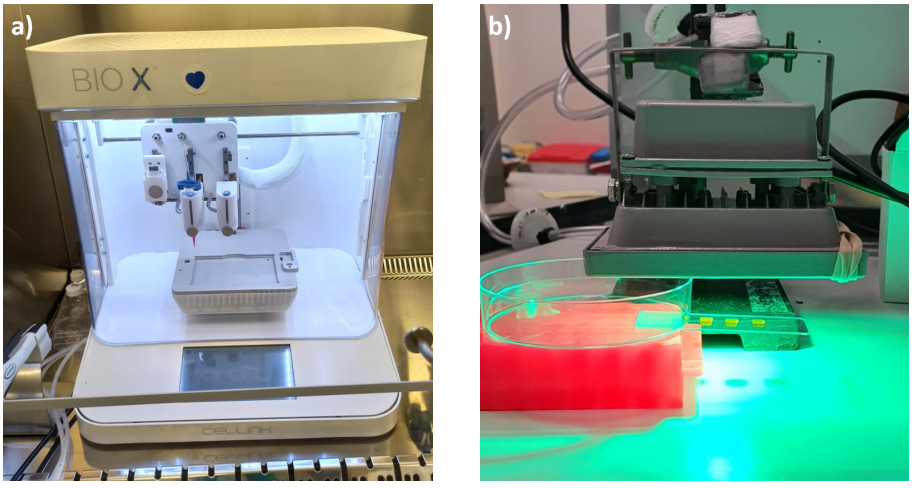

(a) (b)

Figure 2.2: The bioprinting setup. (a) Bioprinter in cell culture hood. (b) Photo-crosslinking of samples with green light at a distance of 2 cm.

2.8. Bioprinting

For this thesis, we have bioprinted cells twice. A preliminary bioprinting test was performed to see if the bioink would be biocompatible with the hMSC and if the cells would survive the printing process. The second time was the final bioprinting with bioinks including THA and a varying concentration of AC dECM. For the bioprinting test, only the $THA_{2.5}$ bioink was prepared. The bioprinting procedure was carried out exactly as described be-

low, except that PBS was used to prepare the bioinks instead of expansion medium, 0.25 mM H_2O_2 was used for enzymatic crosslinking, and 3 x 10 cells/ml (passage 3) were mixed into the ink.

For bioprinting three bioinks were prepared: $THA_{2.5}$, $THA_{2.5}$-$AC_{0.5}$, $THA_{2.5}$-AC_1). The bioink containing THA serves as a control to compare the addition of AC dECM. The cell-laden bioinks were prepared as described in Section 2.7 with the following compositions: 2.5% w/v THA, 0.0%-1.0% w/v AC dECM, 0.1 U/mL HRP, 0.01% w/v EO, 0.3 mM H_2O_2 and expansion medium to reach the desired composition. The hMSCs used for bioprinting were at passage 4 and prepared as reported in Section 2.5. Subsequently, cells ($5x10^6$ cells/ml, resuspended in expansion medium) were mixed with the bioinks by using two syringes (luor lock connection). Slowly homogenizing the bioink by mixing the bioink back and forth between two syringes. To remove air bubbles caused by the mixing, the bioinks were centrifuged for 5' at 200g, concentrating the bubbles at the top, which were subsequently removed by pushing them out of the syringe. Next, the bioinks were loaded in a sterile autoclaved cartridge to start bioprinting.

In order to initiate the bioprinting process, first the printer set up was sterilized to make sure the bioprinting would happen under sterile conditions. A two step sterilization procedure was executed, to begin the outside of the printer was cleaned with 70% ethanol and moved to a cell culture hood. The printer and the inside of the hood were sterilized by turning on the UV-light of the hood for 15'. Secondly, the inside of the printer was sterilized by initializing the 'clean chamber' option, which employs UV-light and hepa filter system for cleaning the air in the bioprinting chamber. After the sterilization was completed, the scaffold design was loaded into the printer. For the scaffolds, a 5 mm x 5 mm x 2 mm (LxWxH) grid structure was created, with a layer height was 0.25 mm and a filament width of 0.8 mm. Next, the cartridge was loaded into the printer and the printing parameters (nozzle size, pressure, syringe size and printing speed) were selected. The scaffolds were printed on a glass slide with a 25G nozzle, a printing speed of 5 mm/sec and and pressures between 65-75 kPa. After extrusion, the structures were further crosslinked with green visible light for 10' (5' top of scaffold and 5' bottom of scaffold). Thereafter the scaffolds were transferred to 24 well plate with 2 ml of expansion medium. After one day, the cell were refreshed and the medium was changed to chondrogenic differentaion medium. The chondrogenic differentation medium was changed two times a week, adding 2 ml to every well. In total, six scaffolds were bioprinted for each time point (t=1, t=7 and t=28). Per time point three scaffolds were used for PrestoBlue/Histological analysis and three scaffolds were used live/dead (L/D) analysis, swelling and mechanical testing (see Table 2.3). A graphical overview of the bioprinting process and scaffold characterizations are presented in Fig. 2.3.

Table 2.3: Overview of experimental studies with cells, displaying the amount of scaffolds used for each time point and which analyses were performed (live/dead (L/D), compression test, swelling, PrestoBlue, histology).

	Total samples	**Tests**	**Day 1**	**Day 2**	**Day 4**	**Day 7**	**Day 8**	**Day 28**
$THA_{2.5}$ (Bioprinting)	n=16	Compression test L/D and Swelling			2	3		3
		PrestoBlue Histology	2			3		3
$THA_{2.5}$-$AC_{0.5}$ (Bioprinting)	n=18	Compression test L/D and Swelling			3	3		3
		PrestoBlue Histology	3			3		3
$THA_{2.5}$-AC_1 (Bioprinting)	n=18	Compression test L/D and Swelling			3	3		3
		PrestoBlue Histology	3			3		3
$THA_{2.5}$ (Molding study)	n=6	L/D		3			3	
$THA_{2.5}$-AC_1 (Molding study)	n=6	L/D		3			3	
Pellet study	n=3	Histology						3

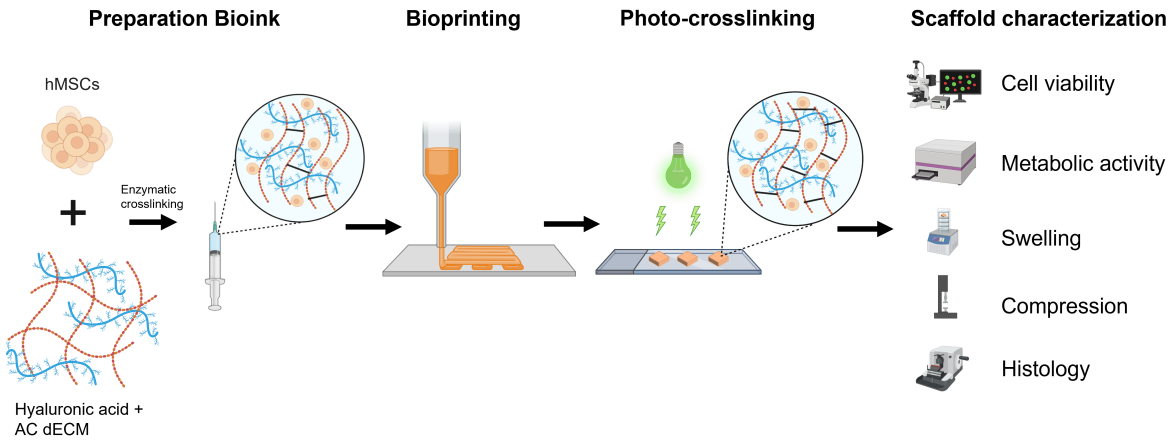

Figure 2.3: Graphical overview of the bioprinting process and scaffold characterization.

2.9. Live/dead

The cell viability of the constructs were assessed by using the Invitrogen Live/Dead TM Viability/Cytotoxicity Kit. The kit contains two stainings: green-fluorescent calcein-AM, for the life cells, and red-fluorescent ethidium homodimer-1, to indicate dead cells. Calcein-AM is a membrane permeable and non fluorescent compound that, once absorbed by liv-

ing cell, is converted to the green fluorescent, membrane-inpermeant calcein, which is retained in the cytoplasma of live cells. Ethidium homodimer-1 is a membrane impermeable fluorescent dye, which becomes strong fluorescent when it binds to DNA. For living cells the dye cannot enter the cell, but when cells die the disrupted cell membrane allows the ethidium homodimer-1 to enter the cells. Sometimes cells can be red and green at the same time, when cells membrane has been damaged, for example during late apoptosis. The cell membrane is still partly intact, allowing both dyes to be present.

The protocol of the L/D staining start with the removal of medium. Subsequently, scaffolds were washed 2 times for 5' in PBS. The washed scaffolds were then incubated with 2 mM calcein-AM and 4 mM Ethidium homodimer-1 in PBS for 30' at 37 degrees. After incubation, the reagents solution was discarded and the scaffolds were transferred to PBS. For imaging, the scaffolds were transferred to a glass slide (Menzel-Glaser Superfrost, ThermoScientific) and imaged with a fluorescent microscope (ZOE fluorescent cell imager, Biorad). Three L/D pictures per scaffolds were used to quantify the cell viability by counting the live cells (green) and dead cells (red) with ImageJ software. Moreover, the circularity of the cells was measured using ImageJ software.

2.10. PrestoBlue

The metabolic activity of the cells within the bioprinted scaffolds was evaluated using PrestoBlue assay (ThermoFisher). PrestoBlue is a reagent that can give an indication of the cell viability by using the metabollic activity of living cells. The PrestoBlue reagent is a resazurin based solution, that is a cell-permeant , blue in color and non-fluorescent. Upon entering the cell, resazurin is reduced to resorufin by metabolically active cells, turning into a red highly fluorescent dye. This conversion is proportional to the amount of metabolically active cells and can be quantitatively measured by using fluorescence detection. For this assay the scaffolds were transferred to a fresh culture medium supplemented with 10% PrestoBlue reagent and incubated for 60' at 37 degrees. Afterwards, 100 µl of the incubated medium was transferred to a 96 well plate (n=2) to measure the fluorescence using a microplate reader (PerkinElmer, Massachusetts, US). For the protocol an excitation of 530nm and emission of 570nm with 0.5s sample time was employed. Wells containing only culture medium with 10% PrestoBlue reagent were used as control to measure the background fluorescence. The background noise was subtracted from the experimental wells.

2.11. Compression test

The compression modulus of the scaffolds was determined by using an unconfined compression test. The test was performed using a Compression Test Stand(ESM303, Mark 10) fitted with a 2.5 N load, a lowering speed of 0.2 mm min^{-1} and sample frequency of 5 measurement per minute. For the compression test, an unconfined load was applied to the scaffold until a certain displacement was reached on the scaffold. The results of these measurement were used to calculate the stress and strain. The relationship between the stress and strain is subsequently used to calculate the compression modulus. A picture of the compression test setup can be seen in Fig. 2.4.

$$\sigma = \frac{F}{A} \tag{2.1}$$

$$\epsilon = \frac{\Delta L}{L_0} = \frac{L - L_0}{L_0} \tag{2.2}$$

The data set obtained from the compression test included the applied load (N) and travel distance of the upper plate(mm) for every reading. To determine the compression modulus, first the stress (σ) is calculated by dividing the applied load (F) by the area (A), expressed in Eq. (2.1). The area (in mm^2) of the scaffolds was determined by multiplying the length and width of sample. Next, the strain was calculated, using the height of the sample (L_0) and the length after deformation (L), by dividing the change in length ($\delta L = L - L_0$) by L_0, given in Eq. 2.2. The stress and strain were calculated for every reading of the measurement. The compression modulus was calculated by fitting the stress/strain curve from 0.0% to 20% strain using linear regression in MATLAB.

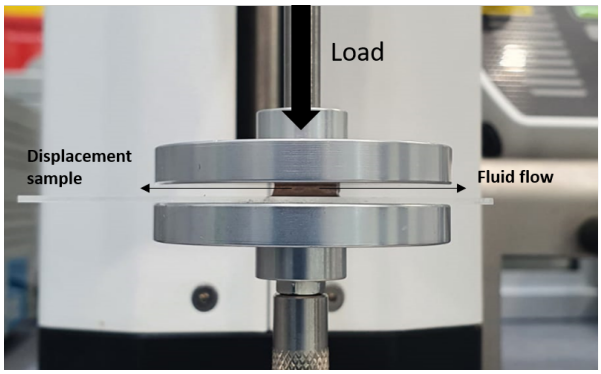

Figure 2.4: Setup of the Mark 10 used for mechanical compression tests of scaffolds.

2.12. Swelling

To assess the water retention capacity of the printed scaffold the swelling ratio was calculated. The swelling ratio was calculated with two different methods, both using the weight of the printed scaffold. For the scaffolds printed without hMSCs, the swelling ratio was determined by measuring the weight of the swollen construct at different time points (W_t) and the weight of the construct immediately after printing (W_0), expressed in Eq. 2.3.

$$\text{Swelling ratio} = \frac{W_t - W_0}{W_0} \tag{2.3}$$

For the bioprinted scaffolds (with MSCs), the swelling ratio was calculated by measuring the weight of the swollen construct for different time points ($W_{swollen}$), t=1, t=7 and t=28, and the dry weight of the construct (W_{dry}), expressed in Eq. 2.4. For the swollen scaffolds, the swollen weight of the scaffolds was measured after L/D analysis. The same sample were subsequently used for mechanical testing and immediately after frozen in the -80°C freezer. The next day, the samples were freeze dried (Alpha 1-2 LDplus, Christ) for 24 hours under vacuum to obtain the dry weight.

$$\text{Swelling ratio} = \frac{W_{\text{swollen}} - W_{\text{dry}}}{W_{\text{dry}}} \tag{2.4}$$

2.13. Histology

Histology is a technique to reveal the presence or absence of tissue specific molecules and the morphology of cells embedded in the bioprinted scaffolds. The procedure consists of 6 steps: fixation, dehydration, wax-embedding, slicing, staining and imaging. Histology was performed for the pellet study and bioprinted scaffolds.

2.13.1. Fixation

The scaffolds used for histology were harvested at day 1, day 7 and day 28 after the Presto Blue analysis was performed. To get rid of the blue dye, the scaffolds were washed with 1x PBS for 2 hours under rotation (4 rpm). The first step, fixation, is executed to preserve the tissue and cells as close as possible to the living state. The samples were fixed overnight at 4°C with 1 ml solution containing: 2% w/v PFA, 2.5% w/v Glutaraldehyde, 0.5% w/v cetylpyridinium chloride (CPC) and 0.03 M NaCl dissolved in 1x PBS. The next day the samples were washed twice with 1x PBS, placed in fresh PBS and stored in the fridge (4°C) until further process.

After 21 days of culture, the pellets were fixed using 4% PFA overnight under rotation (4 rpm). Following that, the pellets were washed twice with PBS and stored in the refrigerator (4° C) until further processing. Before starting the dehydration step, the pellets were embedded in 3% agarose.

2.13.2. Dehydration and Wax-embedding

After fixation all scaffolds were cut through the middle into two parts. One half of each scaffold was used for histology and stored in labeled cassettes used for the dehydration process. During this process all the water is removed from the scaffold. This step is essential as preparation for the embedding with paraffin wax, since paraffin is not miscible with water. The samples were dehydrated through a graded ethanol solutions (70% EtOH, 80% EtOH, 90% EtOH and 2x 100% EtOH) and 2 times xylene washing. All the ethanol steps took 60' and each of the xylene washings was 30'. Placing the samples in graded alcohols minimizes the tissue damage and shrinkage. While the samples were dehydrated, the paraffin wax was melted at 80°C. Following the xylene steps, the samples were placed in melted paraffin for 60'.

To perform the embedding, a heating plate was warmed and the samples were retrieved from the wax. The process started by pouring a small amount of paraffin into a metal mold, the sample was placed in the centre of the metal mold and manipulate into the desired orientation. The mold was cooled down to solidify the paraffin, so the sample would stay in position. When the sample was fixed, the cassette bottom of the corresponding sample was heated on the heating plate. The cassette bottom was subsequently placed on top of the sample and hot wax was poured over the sample till the cassette was completely covered. The sample were attached to the cassette bottom for labeling, easy removal from the mold and to be able to slice the sample. The samples, fixed between the mold and cassette, were cool down at room temperature and stored until the next step.

2.13.3. Sectioning

Once embedded, the samples were sectioned into thin slices using the Leica RM2135 microtome with a thickness of 8 µm for bioprinted scaffolds and 6 µm for the pellet study. To begin, the excessive wax was removed by slicing the sample until a Section containing the full sample was observed. Three slices of the full sample were carefully picked up and placed in a warm water bath (50°C, to relax the wax). Relaxation is important to smooth out the wax and regain its original shape. The relaxed slices were picked up with a glass slide (Menzel-Glaser Superfrost, ThermoScientific) and dried overnight at 37°C, causing the slices to stick to the glass slide.

2.13.4. Staining

After drying, the samples were ready for the staining process. Staining is employed to highlight components of interest in the sample. The samples were stained with three stainings: Alcian Blue, Picrosirius Red and Hematoxylin and Eosin (H&E). The staining protocol consists of four parts: hydration, staining, dehydration and mounting.

Alcian Blue

Alcian Blue is a blue colored, positively charged dye and stains sulfated glycosaminoglycans (sGAGs), a major component of the ECM of AC. The positive charge of the Alcian Blue is attracted to the negatively charged sGAGs, staining the sGAGs by forming a strong binding in an acidic environment (pH 1).

The protocol for Alcian Blue starts with the hydration of the sample slides. The slides are immersed twice in Xylene for 5', twice in 100% EtOH for 5', twice in 95% EtOH for 3', once in 70% EtOH for 3' and once in deionised H_2O for 5'. Next, the hydrated samples slides were submerged in Alcian Blue (pH 1) for 5' to stain the sGAGs. Then, the samples are washed 3 times with deionised H_2O for a total of 30 seconds. The samples were stained for a second time with 0.1 % w/v Nuclear Fast Red to visualize the cell nuclei and correspondingly washed for 1' with running tap water and 30 seconds of deionised H_2O. Next, the sample slides where dehydrated with by being immersed twice in 95% EtOH, twice in 100% EtOH and twice in Xylene. All the alcohol steps lasted for 20 seconds and each Xylene step lasted 3'. Immediately after, the slides were mounted with Dibutylphthalate Polystyrene Xylene (DPX, Sigma-Aldrich) and a cover slip. All the slides were dried overnight at room temperature in a chemical hood with circulation flow.

Picrosirius Red

Picrosirius Red stains another important ECM component of AC, namely collagen. This stain is negatively charged and binds to the positively charged collagen fibers. The stained collagen can be imaged with standard light microscopy settings or polarized light to see the difference between different types of collagen. The protocol of the Picrosirius Red staining is similar to the Alcian Blue protocol and start with hydration. The sample were immersed twice in Xylene for 5', twice in 100% EtOH for 5', twice in 95% EtOH for 3', once in 70% EtOH for 3' and once in deionised H_2O for 5'. Next, the hydrated samples slides were submerged in Picrosirius Red for 60' and thereafter washed twice for 30 seconds with 0.5% acetic acid. Then, the sample slides where consecutively dehydrated by being immersed twice in deionised H_2O for 30", twice in 95% EtOH for 20 seconds, twice in 100% EtOH for

20 seconds and twice in Xylene for 3'. Immediately after, the slides were mounted with Dibutylphthalate Polystyrene Xylene (DPX, Sigma-Aldrich) and a cover slip.

Hematoxylin and Eosin
The tissue and cell morphology was checked with an H&E staining. Hematoxylin stains the cell nuclei in a purplish/blue color and Eosin stains the ECM and the cytoplasm pink. Comparatively to the Alcian Blue and Picrosirius Red, the HE staining protocol starts with hydration. The sample slides were immersed twice in Xylene for 5', twice in 100% EtOH for 5', twice in 95% EtOH for 3', once in 70% EtOH for 3' and once in deionised H_2O for 5'. Next, the hydrated samples slides were submerged in Harris Hematoxylin for 4', thereafter washed with running tap water for 10' and 5 dibs in the acid alcohol (1 µl HCL in 400 µl of 70% EtOH. Harris Hematoxylin was filtered before use through Whatman filter paper. The samples were again washed in tap water for 5' and subsequently stained for 2' with eosin. Then, the sample slides where consecutively dehydrated by being immersed twice in 95% EtOH, twice in 100% EtOH and twice in Xylene. Each step lasted 3'. Immediately after, the slides were mounted with Dibutylphthalate Polystyrene Xylene (DPX, Sigma-Aldrich) and a cover slip.

2.13.5. Imaging
The stained samples slides were imaged under a DM500 optical Leica microscope with 70% brightness, saturation of 100, gamma of 0.7 and 1 gain. An overview image of every sample was composed of by combining multiple pictures taken with a 4x objective. In addition, close up images of very sample were taken with a 40x objective.

2.13.6. Image analysis
To quantify the production of sGAGs and collagen, histology images of Alcian Blue and Picrosirius Red staining were analysed using ImageJ software. For the quantification three close up images of each sample, taken with the 40x objective, were evaluated. The microscope images were split into three color channels (red, green and blue). The green channel was used for further analysis because it was optimal to distinguish the sGAGs/collagen from the rest of the sample. Then, the threshold of the selected channel was adjusted to make the produced sGAGs/collagen even more detectable, creating a black/white image. Finally the percentage of produced sGAGs/collagen was obtained by measuring the area fraction the sGAGs/collagen occupied in the images.

2.14. Statistical Analysis
The data is reported with the mean plus standard deviation with n=3 unless specified otherwise. All statistical analyses were performed using Graphpad Prism (Graphpad software, version 9). An unpaired t-test was used to compare the two groups and the results were considered significant at a level of $p<0.05$. One-way analysis of variance (ANOVA) was used to compare more than two groups, with post hoc testing and significance established at p 0.05. For multiple comparisons, the two-way ANOVA correction was applied with a significance level of $\alpha = 0.05$.

3

Results

3.1. Rheological characterization and printability test of THA

Rheological characterization can be used to predict the printability and the shape fidelity of bioinks. Rheology is the study of flow and deformation of materials as a result of applied forces [29]. In 3D bioprinting, a bioink begins in a bulk resting state, transitions to a high shear condition while passing through the nozzle, takes on a new shape, and then assumes a new resting state. This shape transition is described by four rheological parameters: damping factor, yield stress, shear thinning and recovery.

Table 3.1: Relating the damping factor to the printability and extrudability of the THA inks with varying concentrations of H_2O_2 (0.1, 0.25 and 0.3 mM).

THA w/v	**H2O2 (mM)**	**G' (Pa)**	**G" (Pa)**	**Damping factor**	**Extrudability**	**Printability**
2.5 %	0.1	21.1	13.0	0.616	Yes	Poor (too liquid)
2.5 %	0.25	245	13.8	0.056	Yes	Good
2.5 %	0.3	379	14.7	0.039	Yes	Poor (granular)

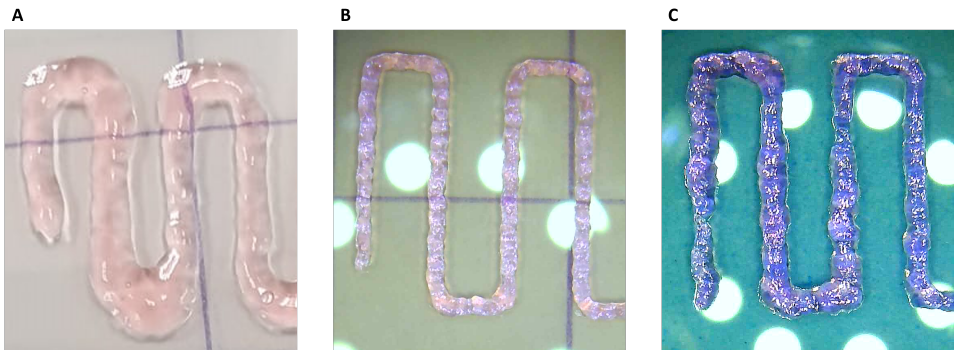

Figure 3.1: Printability of the THA ink with varying concentration of H_2O_2 by reviewing the continuous filament formation. A) THA - 0.1 mM H_2O_2. B) THA - 0.25 mM H_2O_2. C) THA - 0.3 mM H_2O_2.

To identify a printable formulation, the THA ink was crosslinked with varying concentrations of H_2O_2 from 0.1 to 0.3 mM. The damping factor was linked to ink extrusion, by

passing it through a 25G nozzle (extrudability), and shape retention, by printing filaments (printability), shown in Table 3.1. Images of printability are presented in Fig. 3.1. The damping factor was calculated with G' and G " values obtained during a frequency sweep, as shown in Fig. 3.2A. The figure shows that for all concentrations of H_2O_2, G' text is greater than G, indicating elastic behavior. At a concentration of 0.1 mM H_2O_2, the ink was extrudable and had a damping factor of 0.616, but was too fluid to retain its shape after printing. THA with 0.25 mM H_2O_2 had a damping factor of 0.056, was extrudable, and retained shape well. A further increase in the H_2O_2 concentration to 0.3 mM resulted in poor printability and a granular texture in the ink, with a damping factor of 0.039.

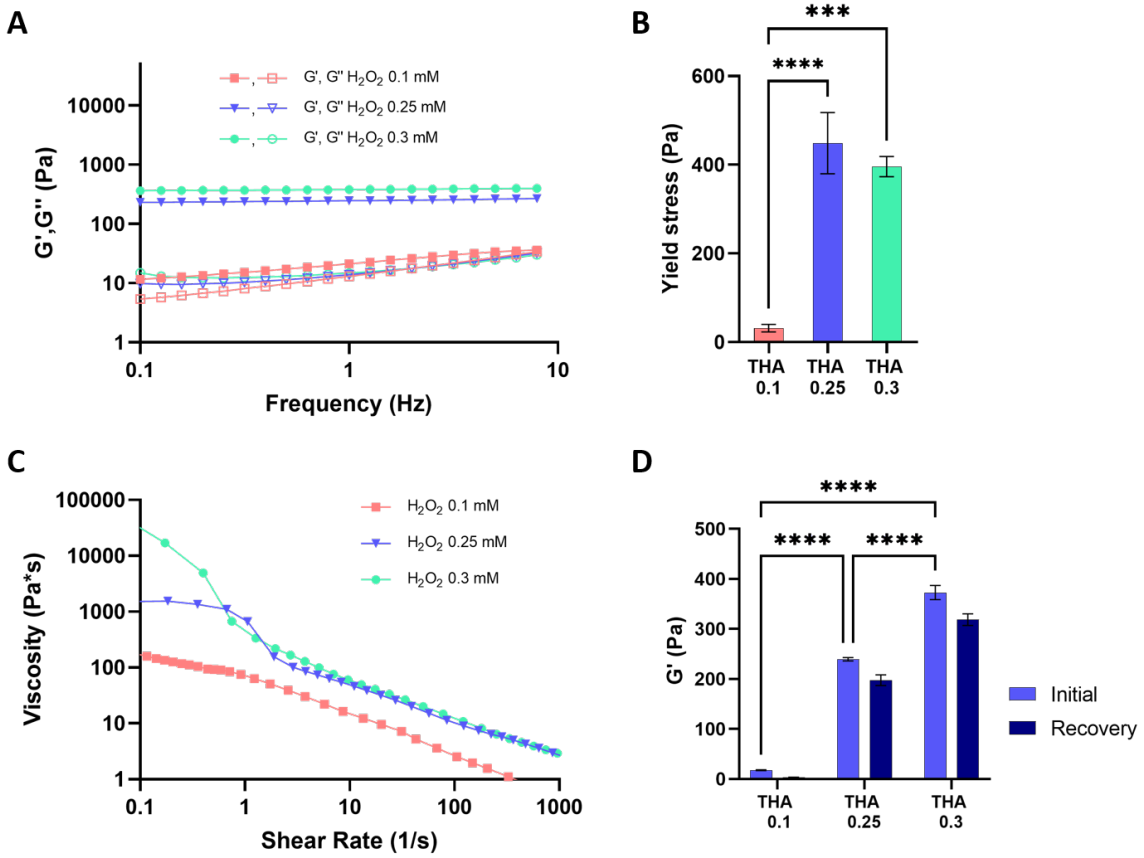

Figure 3.2: Rheological parameters of THA ink with different concentrations of H_2O_2 (0.1, 0.25 and 0.3 mM). A) The G' (closed symbols) and G" (open symbols) as function of the frequency; B) The yield stress determined by measuring the crossover point of G' and G" as a function of the shear stress; C) Plot of viscosity as a function of the shear rate; D) The recovery of the G'.

In Fig. 3.2B the results of the yield stress measurements are presented. The yield stress is the amount of stress that must be exceeded in order for a material to deform [29]. A material will act like a solid below the yield stress, but will flow above it. In addition the yield stress is related the amount of crosslinking within the inks. The yield stress is another important property of a bioink, because it will support suspended cells in a syringe, but will flow as liquid when enough stress is applied. The yield stress is an important parameter, because the yield stress is essential for a material to keep its shape after bioprinting and support the

weight of following layers [11]. For the all the THA inks with varying concentration of H_2O_2 yield stress is present, although for 0.1 mM H_2O_2 the yield is very low. The addition of 0.1 mM H_2O_2 results in a yield stress of 31.6 ± 8.5 Pa. By increasing the H_2O_2 concentration to 0.25 mM, the yields stress increases to 448.9 ± 69 Pa, due to the higher number of crosslinks in the ink. Although a significant difference was observed when the concentration of H_2O_2 increased from 0.1 to 0.25 mM, increasing the concentration of H_2O_2 to 0.3 mM did not result in a significant difference compared to the ink with 0.25 mM H_2O_2.

A common way to investigate the non-Newtonian behavior of fluids is by measuring the viscosity when the shear rate is gradually increased. Wherefore shear thinning behavior, an decrease of the viscosity when the shear rate is increased, is desired for bioink to be extruded through a small nozzle [9]. In bioprinting this test is often used to understand to flow properties of the ink during extrusion, as well as the initial shape preservation after printing [29]. A higher viscosity at zero shear rate means a slower deformation of the material, which can increase the stability of the bioink after printing. The influence of the concentration H_2O_2 on the viscosity was investigated (Fig. 3.2C). All the inks displayed shear thinning behavior, meaning that the viscosity will be reduced during the extrusion and easing the printing process. The THA ink with 0.1 mM H_2O_2 had a viscosity ranging from 171.3 Pa*s at 0.1 s^{-1} and 2.5 Pa at 100 s^{-1}. The viscosity of the THA with 0.25 and 0.3 mM H_2O_2 were more similar, 1515 Pa and 17053 Pa at 0.1 s^{-1} to 9.2Pa and 10.9 Pa at 100 s^{-1}.

The storage modulus recovery gives information about the transition of the fluid to flow to the shape retention of the printing process. The recovery of the inks, after being exposed to stress higher than the yield stress, is presented in Fig. 3.2D. Changing the concentration of H_2O_2 caused a significant increase in the G', reaching a G' of 17.6 ± 0.8 Pa for 0.1 mM, 239.5 ± 3.4 Pa for 0.25 mM and 372.8 ± 14.3 Pa for 0.3 mM. Also, a difference in the recovery was observed in all inks. The ink formulation containing 0.1 mM H_2O_2 yielded a recovery of 20.8 ± 2.4.The recovery for the increased concentration of H_2O_2, 0.25 mM and 0.3 mM, was significantly higher, $81.5 \pm 4.5\%$ and $85.6 \pm 0.4\%$.

Based on the above characterizations, it can be concluded that only the THA ink with a concentration of 0.25 mM is printable. The use of 0.1 mM and 0.3 mM resulted in poor printability, which could also be determined from the viscosity measurement. A significantly lower viscosity for the 0.1 mM and a higher viscosity for the 0.3 mM, compared to the 0.25 mM H_2O_2 bioink. In addition, a very low recovery was found for the 0.1 mM H_2O_2 bioink, which confirmed the fluid behavior and poor shape retention, visible in Fig. 3.1A.

3.2. Development of the THA-AC bioinks

Based on the results of the previous section's analysis, the $THA_{2.5}$ ink with 0.25 mM H_2O_2 was chosen for the remainder of the study. Next, for the selected $THA_{2.5}$ ink, the influence of the AC dECM addition was tested by performing rheological analysis, presented in Fig. 3.4.

Table 3.2: Relating the damping factor to the extrudability and printability of a THA ink with varying concentrations of AC (0%, 0.5% and 1%)

THA w/v	AC w/v	H2O2 (mM)	G' (Pa)	G" (Pa)	Damping factor	Extrudability	Printability
2.5 %	0.0 %	0.25	245	13.8	0.056	Yes	Good
2.5 %	0.5 %	0.25	156	18.3	0.117	Yes	Good
2.5 %	1.0 %	0.25	160	22.5	0.140	Yes	Good

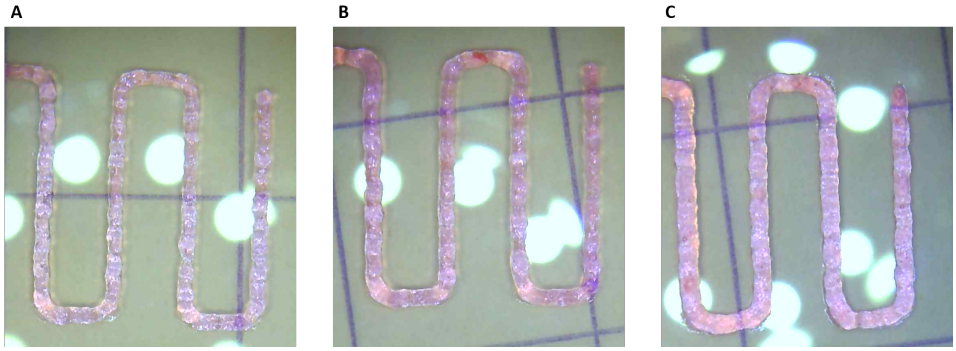

Figure 3.3: Printability of the THA-AC inks with varying concentration of AC. Determined by reviewing the continuous filament formation. A) $THA_{2.5}$. B) $THA_{2.5}$-$AC_{0.5}$. C) $THA_{2.5}$-AC_1.

The influence of AC dECM addition on the viscoelasticity of the inks can be seen in Fig. 3.4A. The change in damping factor and its relation to extrudability and printability are presented in Table 3.2 and Fig. 3.3. For all the ink formulations G' >G", indicating elastic behavior of the inks. By combining $THA_{2.5}$ with varying concentrations of AC dECM, the G' significantly decreased from 245 Pa ($THA_{2.5}$)to 156 Pa ($THA_{2.5}$-$AC_{0.5}$) and 160 Pa ($THA_{2.5}$-AC_1). This decrease also affected the damping factor, which in contrast increased from 0.056 to 0.117 and 0.141. Even though the damping factor was increased, the inks with AC were still extrudable and had good printability.

For the yield stress, a significant difference was observed when AC dECM was added to the ink composition (Fig. 3.2B). When AC dECM was combined with THA, the yield stress increased from 448.9 ± 69Pa for $THA_{2.5}$ ink to 602.1 ± 27 Pa for $THA_{2.5}$-$AC_{0.5}$ and 567 ± 20 Pa for $THA_{2.5}$-AC_1. There was, however, no significant difference between the different AC dECM concentrations.

Moreover, the effect of AC dECM on the viscosity of $THA_{2.5}$ ink was investigated (Fig 3.2A). The ink without AC dECM showed shear-thinning behavior with a decrease in the viscosity from 1515 Pa*s at 0.01 s^{-1} to 9.2 Pa*s at 100 s^{-1}. Comparatively, the inks with the addition of AC show shear-thinning behavior. The low shear rate viscosity, on the other hand, is

higher, ranging from 1993 Pa*s for $THA_{2.5}$-$AC_{0.5}$ and 5126 Pa*s for $THA_{2.5}$-$AC_{0.5}$ at 0.01 s^{-1} to 7.8 Pa*s and 9.3 Pa*s at 100 s^{-1}. Increasing the shape retention abilities of the inks with the addition of AC dECM. Furthermore, all three inks had a recovery rate greater than 85%, where G' recovery was 85.6 % ($THA_{2.5}$),87.4% ($THA_{2.5}$-$AC_{0.5}$) and 85.8% ($THA_{2.5}$-AC_1)

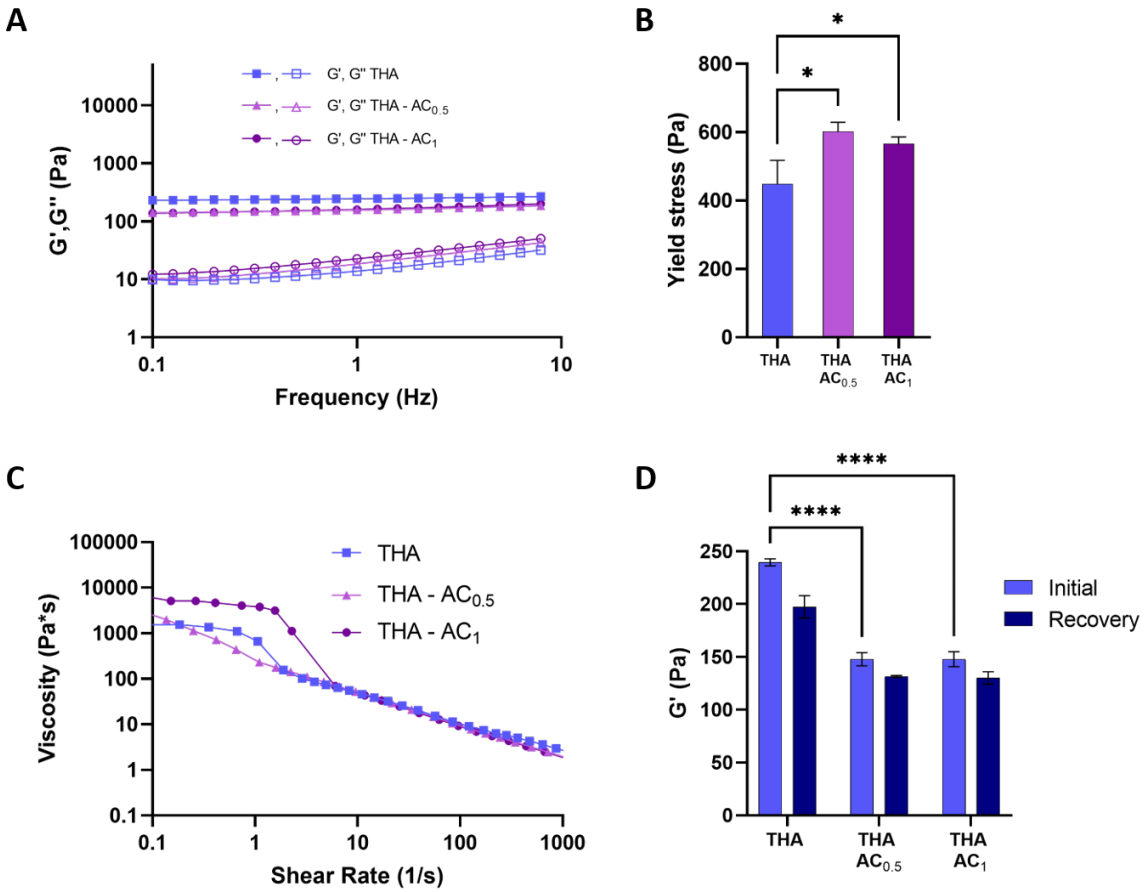

Figure 3.4: Rheological parameters of THA ink with different concentrations of AC dECM (0%, 0.5% and 1% w/v). A) The G' (closed symbols) and G" (open symbols) as function of the frequency; B) The yield stress determined by measuring the crossover point of G' and G" as a function of the shear stress; C) Plot of viscosity as a function of the shear rate; D) The recovery of the G'.

3.3. Optimization of the photo-crosslinking process

The influence of the pressure, nozzle size and printing speed on filament formation was determined by characterizing the filament width for the inks ($THA_{2.5}$, $THA_{2.5}$-$AC_{0.5}$ and $THA_{2.5}$-AC_1, presented in Appendix A.1. This optimization resulted in the following printing settings for the $THA_{2.5}$ ink: a 25G nozzle with 40 kPa pressure and a speed of 7 mm/s. These optimized parameters were applied to the printing of a square scaffold, 5 mm x 5 mm x 2.4 mm (L x W x H) with 8 layers (Fig. 3.5A). The construct has a rectilinear pattern with 7 fibers for each layer. A picture of the printed scaffold can be seen in Figure 3.5C.

For the printed scaffold, it was observed that the enzymatic pre-crosslinking is not sufficient for post-printing shape fidelity. Without additional stabilization, the printed constructs collapsed and almost doubled in size after one day in PBS (Fig. SA.5). Therefore, the printed structures were further crosslinked with exposure to green light. To obtain the optimal printing conditions, the effect of the light crosslinking time and the position of the scaffold compared to the green light source were tested. Exposing the scaffolds to green light only from the top could cause inconsistent crosslinking throughout the scaffold. The influence of green light was assessed by looking at the shape of the scaffold and measuring the swelling and compression modulus.

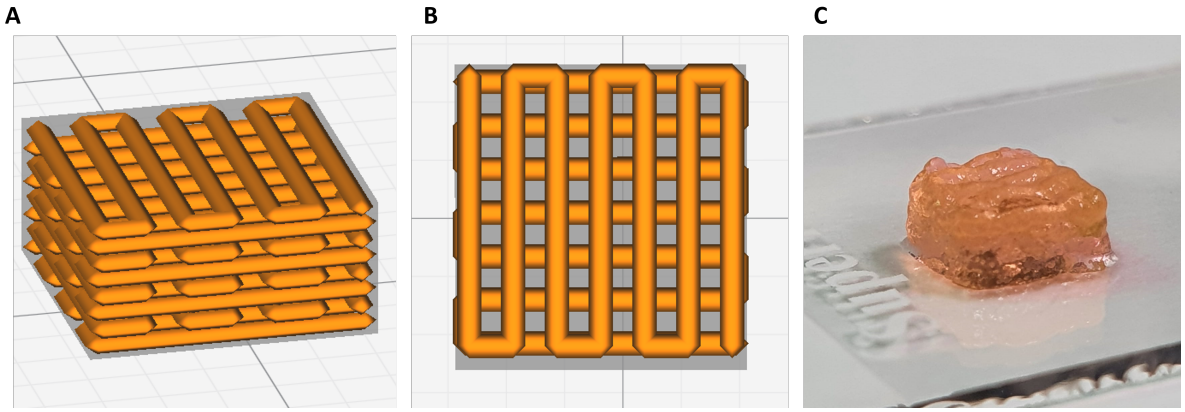

Figure 3.5: Design of the printed scaffold with 8 layers in a rectilinear pattern. A) Isometric view. B) Top view. C) Isomtric view of the printed scaffold.

Scaffolds were photo-crosslinked for 5' or 10' with green light exposure only from the top side (without turning) or from both sides (with turning of the transparent slide) (Fig 3.6A). The influence of light exposure on shape retention is shown in Fig. 3.6B. We observed that scaffolds with only light exposure from the top did not retain their structure on the bottom side. Whereas, the shape of the scaffolds, which were turned halfway through time, was better preserved. The swelling was measured after 24 h for all conditions, presented in Fig. 3.6C. For the scaffold exposed to 5' of green light, a significant difference was noted when the scaffolds were turned or not. The swelling ratio for scaffolds with light exposure only from the top side was 1.39, higher than the ones with light exposure from both sides, 1.27. An increase in the green light exposure to 10' further decreased the swelling ratio of the scaffold. This shows the importance of the photo-crosslinking time and, consequently, the crosslinking density on the swelling. No significant difference in the swelling ratio was observed between the scaffold photo-crosslinked for 10' with or without turning.

A similar trend was measured for the compression modulus of the scaffolds (Fig. 3.6D). By increasing the green light exposure from 5' to 10', the network became more crosslinked, resulting in a higher compression modulus. Crosslinking the scaffold only from the top of the scaffold or on both sides does not influence the compression modulus. By photo-crosslinking with green light at 10' and turning the scaffold midway, the scaffold with the best preserved shape was obtained. Hence, these optimized settings were applied to bio-printing.

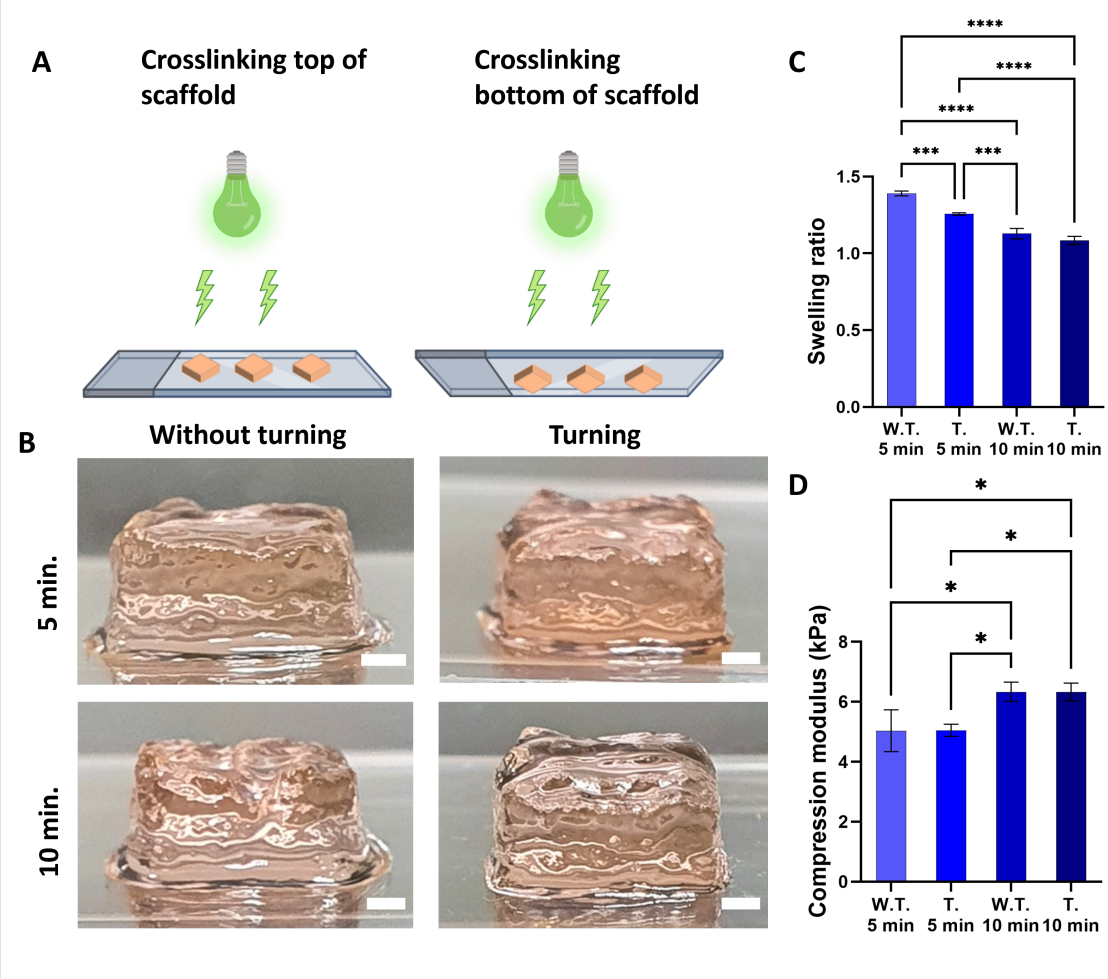

Figure 3.6: The influence of the photo-crosslinking time for 5' and 10' on the printed scaffolds with green light exposure from the top side (without turning) or from both sides (with turning of the transparent slide). The abbreviation in graphs are: without turning 5' (W.T. 5 min), turning 5 min (T. 5 min), without turning 10' (W.T. 10 min) and turning 10' (T. 10 min). A) Graphical overview of scaffolds with light exposure from top and bottom by turning the slide. B) Side view of printed scaffolds, showing the shape retention. Scale bar = 1 mm. C) Swelling ratio calculated by measuring the weight immediately after printing and after one day in PBS. D) The compression modulus.

3.4. Bioprinting test with PBS

Following the optimization of the ink printability and shape retention, a printing test was performed to ensure the viability of the hMSCs throughout the bioprinting process. A $THA_{2.5}$ bioink with 3 x 10^6 cells/ml was printed and was evaluated by using L/D analysis on day 1 and day 7. L/D images after day 1 showed that the cells were colored green as well as red, indicating that the cells were dying (Fig. 3.7A). When cells are in late apoptosis, the cell membrane is still partly intact, allowing both dyes, Calcein and Ethidium homodimer-1 to enter and stain the cells. The L/D analysis of day 7 showed that no cells were alive (Fig. 3.7B). The cell death was most likely caused by the presence of EO in the bioink. EO is used as a photo-initiator for photo-crosslinking, but it can be cytotoxic when it is internalized into the cells. Similar findings were reported in another paper that combined EO and PBS in a bioink, where cell viability decreased from 60% at 10' after printing to 0% after 60' [17]. It was suggested that, due to the lack of proteins that help maintain intracellular homeostasis and the experience of cellular stress, EO had the chance to penetrate the cell. Moreover, the paper proved that by replacing PBS with FBS, the cell viability was still over 90%.

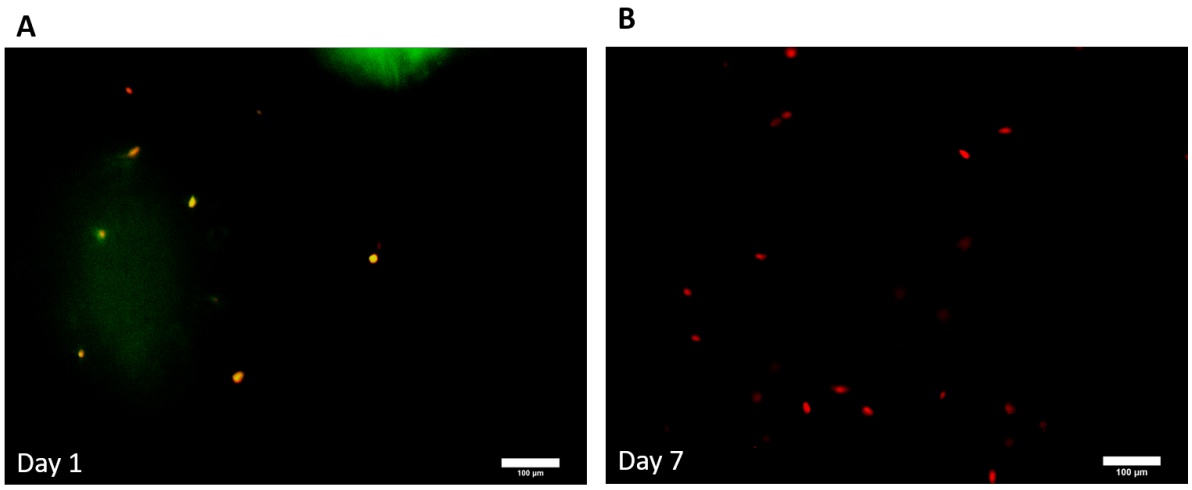

Figure 3.7: L/D images of $THA_{2.5}$ scaffolds with 3x10^6. Scale bar = 100 µm A) Day 1. B) Day 7.

3.5. Influence of bioink composition on hMSCs viability

To test the influence of the bioink compositions on cell viability, hMSCs were encapsulated within the hydrogels and their viability was investigated for 8 days. For this analysis, the hydrogels were not printed, so only the effect of the materials was taken into account. Because the cells died as a result of the initial bioink composition, the PBS was replaced with expansion medium, containing FBS. The viability of the two hydrogel compositions, $THA_{2.5}$ and $THA_{2.5}$-AC_1, were measured over time (Fig. 3.8).

The L/D staining showed live cells (green) and dead cells (red) after 2 and 8 days of culture. The $THA_{2.5}$ hydrogel had a viability of 64.7% for day 2, which slightly increased for day 8 to 72.7%. On day 2, the $THA_{2.5}$-AC_1 hydrogel had 65.9% viability, which remained constant on day 8 with 67.7% viability. Furthermore, we noticed that hMSCs embedded in the $THA_{2.5}$-AC_1 hydrogel showed a more elongated shape at day 8, whereas the cells embedded in the $THA_{2.5}$ hydrogel maintained a round morphology (Fig. 3.8C). Because of the observed cell spreading, it was decided to perform actin staining on the remaining samples on day 10. The images and method of the actin-nuclei staining are presented in Appendix A.5. This staining also indicated that the cells are more spread in the $THA_{2.5}$-AC_1 hydrogel compared to the $THA_{2.5}$ hydrogel.

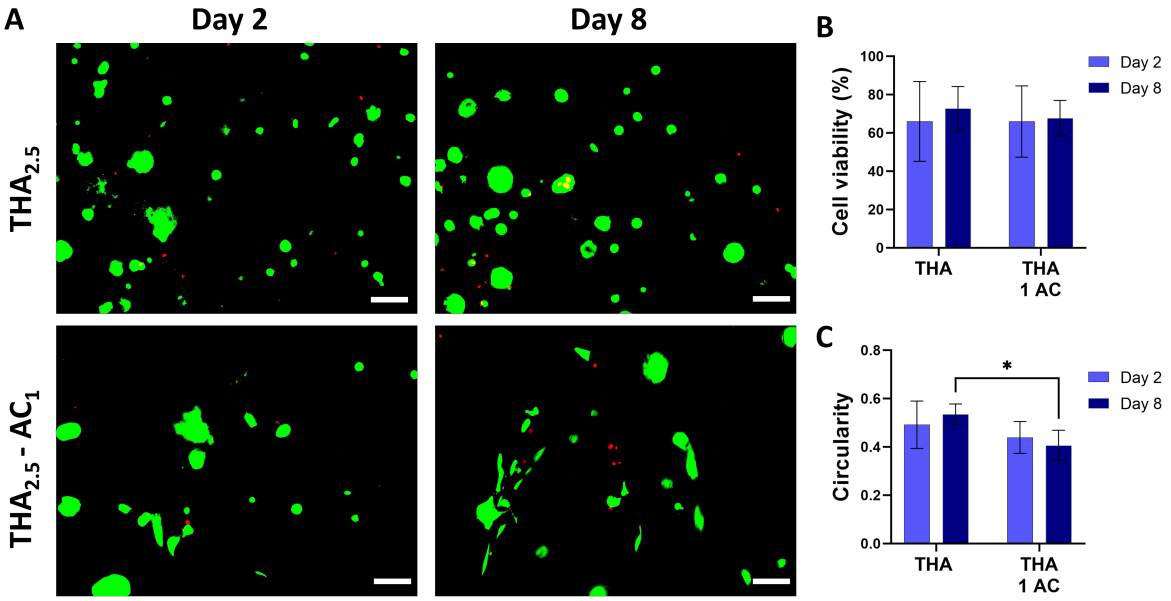

Figure 3.8: Viability of hMSC embedded in a $THA_{2.5}$ and $THA_{2.5}$-AC_1 after 2 and 8 days in culture. A) L/D images. Scale bar = 100 µm B) Cell viability. C) Circularity of hMSCs.

3.6. Bioprinting of hMSCs with THA-AC bioinks

The addition of the expansion medium (containing FBS) to the bioink composition improved the cell viability, but at the same time, it changed the viscoelastic properties of the bioink. For the first bioprinting test, we had already observed that the addition of cells made the bioink a bit more sticky, but it was still printable. However, when the bioink composition changed by substituting PBS with expansion medium, the bioink became too liquid and sticky to be printed. Therefore, the H_2O_2 concentration was increased to 0.3 mM. Moreover, the printing properties were changed to a speed of 5 mm/s with a pressure varying from 65 to 75 kPa for the bioinks.

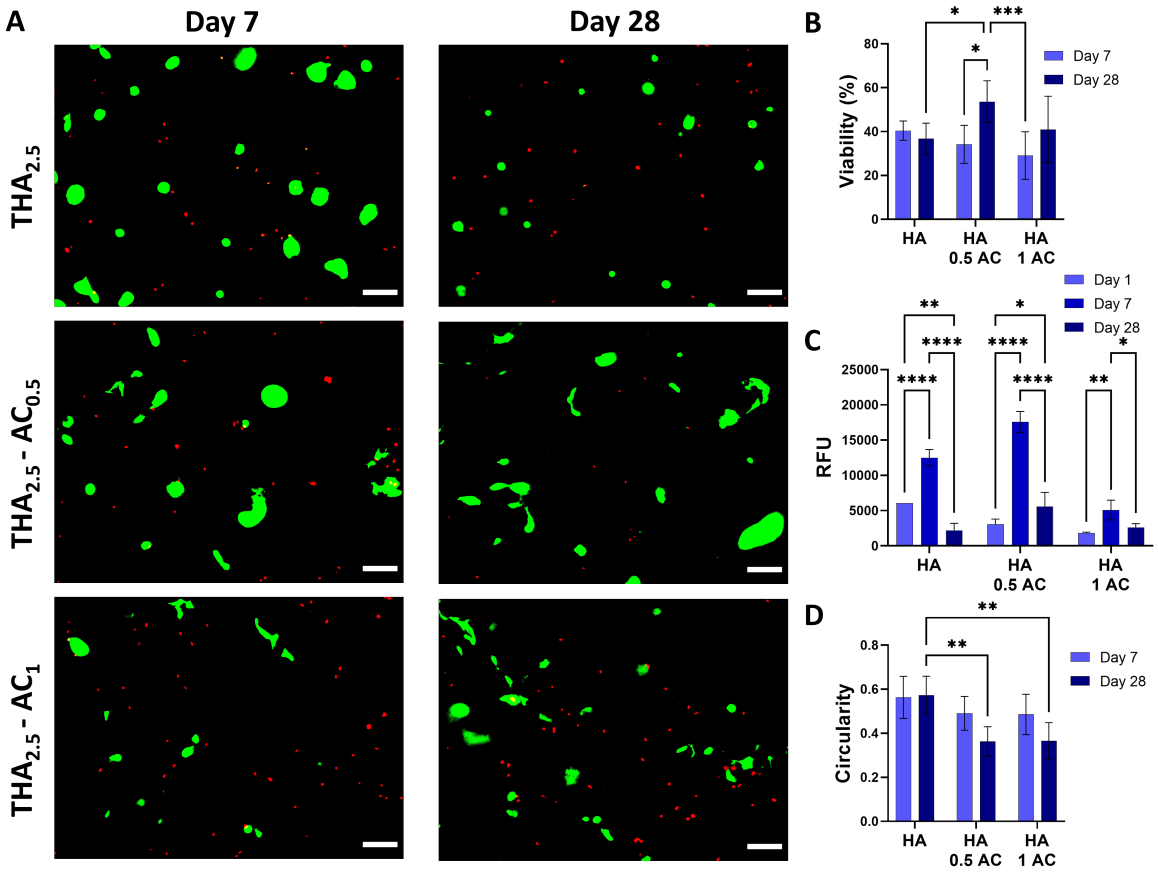

Figure 3.9: Cell viability of scaffolds bioprinted with $THA_{2.5}$, $THA_{2.5}$-$AC_{0.5}$ and $THA_{2.5}$-AC_1 and cell density of 5 x 10^6 cells/ml A) L/D images for day 7 and 28. Scale bar = 100 µm B) Quantification of cell viability based on L/D staining. C) Presto Blue assay for day 1, 7 and 28 in relative fluorescence units (RFU). D) Circularity of the live cell based on L/D staining.

L/D analysis of the bioprinted scaffolds was performed on day 1, day 7 and day 28. However, on day 1, the cells were stained green as well as red, making it difficult to count the cells and determine their viability. As a result, these images are excluded in the results and presented in the Fig. A.6. The cell viability on day 7 was 40.4 %, 34.2 % and 29.1 % for the $THA_{2.5}$, $THA_{2.5}$-$AC_{0.5}$ and $THA_{2.5}$-AC_1 scaffolds (Fig. 3.9A and 3.9B). After 28 days of culture, the cell viability (36.7 %) was preserved for the $THA_{2.5}$ scaffold. Simultaneously, an increase was observed for the $THA_{2.5}$-$AC_{0.5}$ and $THA_{2.5}$-AC_1 scaffold, to 53.6 % and 40.9 % viability. In addition also a difference in the cell viability in the middle and sides of the scaffold was

observed, by cutting the samples in half (Fig. SA.7). The cell viability in the middle of the samples was significantly higher, 83.7%, compared to the sides of the samples, 48.1%.
The PrestoBlue assay indicated an increase in fluorescence intensity on day 7 as compared to day 1 for all scaffolds. Even though the cell viability remained constant or increased on day 28, the fluorescence intensity for all scaffolds significantly decreased on day 28 compared to day 7. A surprising result is the higher fluorescence intensity of the $THA_{2.5}$-$AC_{0.5}$ scaffold on day 7. Furthermore, the hMSCs showed an elongated shape for the scaffold with AC dECM addition. However, the cells embedded in the bioink with only $THA_{2.5}$ maintained a round morphology. On day 28, increasing the concentration of AC from 0.5% w/v to 1% w/v had no effect on the circularity of the cells.

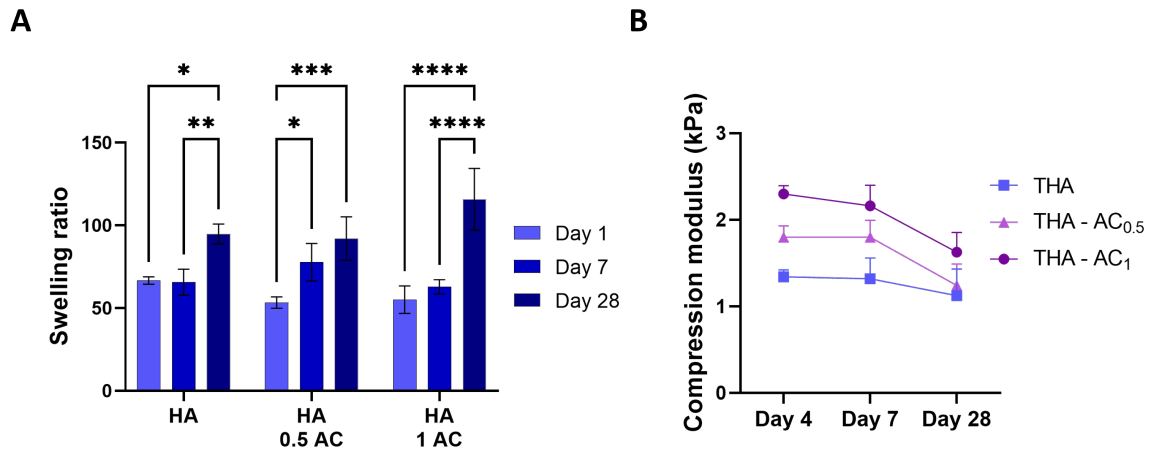

Figure 3.10: Swelling ratio and compression modulus of the cell-laden scaffolds printed with $THA_{2.5}$, $THA_{2.5}$-$AC_{0.5}$ and $THA_{2.5}$-AC_1 and cell density of 5 x 10^6 cells/ml. A) Swelling ratio. B) Compression modulus.

Besides checking the cellular performance of the scaffold, we also measured the physical properties (swelling ratio and compression modulus) of the scaffolds. On day 1 and day 7, the swelling ratio for all scaffolds was approximately 60 (Fig. 3.10A). After 28 days, a significant increase in the swelling ratio was observed for all scaffolds. The compression modulus of the bioprinted scaffold was measured at day 4, 7 and 28, presented in Fig. 3.10B. On day 4, higher compression moduli were observed for scaffolds with AC dECM incorporation compared to scaffolds with only THA. Furthermore, the compression modulus for the $THA_{2.5}$-AC_1 scaffold was greater than that of the $THA_{2.5}$-$AC_{0.5}$ scaffold. The compression moduli were 1.3 kPa for $THA_{2.5}$, 1.8 kPa for $THA_{2.5}$-$AC_{0.5}$ and 2.3 kPa for $THA_{2.5}$-AC_1. On day 7, the compression modulus of all scaffolds remained constant.After 28 days of culture, a decrease was observed for all scaffolds and had comparable compression moduli, 1.1 kPa for for $THA_{2.5}$, 1.2 kPa for $THA_{2.5}$-$AC_{0.5}$ and 1.6 kPa for $THA_{2.5}$-AC_1.

3.7. Histological analysis of the bioprinted scaffolds

For the histological analysis, the scaffolds were stained with Alcian Blue, Picrosirius Red and H&E. The scaffolds were cultured in chondrogenic differentiation medium for 28 days and sectioned at different time points (day 0, 7 and 28). First a pellet study was performed as a control to provide information about the tissue formation (sGAGs and collagen production) of the cells over time in a 3D environment. HMSCs pellets were cultured with chondrogenic differentiation medium for 21 days before histology was performed. The first batch of cells had a slow proliferation rate, where it took the plated cells two to three weeks before 90% confluency was reached. Moreover, the pellet study showed that there was almost no GAG production after 21 days (Fig. SA.10A). This suggests that the hMSC batch did not differentiate sufficiently into chondrocytes. Therefore, we changed donors and got a new batch of hMSCs. Correspondingly, a new pellet study was performed, for which pellets were analysed on day 2 and day 21 (Fig. SA.10B). This pellet study was executed by a fellow master student, Maria Kalogeropoulou. Compared to the first batch of cells, the pellets for this study stained positive for Alcian Blue and Picrosirius Red, indicative of sGAGs and collagen deposition on day 21.

3.7.1. Alcian Blue

Alcian Blue staining was used to see the amount of sGAG production for the scaffolds over time, shown in Fig. 3.11A. On day 0, all samples were expected to have zero GAG production. However, it can be observed that every sample is already positively stained at day 0. To decrease the background staining by HA, Alcian Blue at pH 1 was utilized for the staining. Only sGAGs are stained at pH 1 and although HA is GAG, it does not contain any sulfate. As a result, less HA background staining was expected. The initial amount can be considered negligible, since this is not produced by the cells. When hMSCs differentiate into chondrocytes, they begin to produce sGAGs, which should result in an increase of the blue intensity with time. At day 28, a visual inspection of the images indicates that there might be sGAG deposition in specific regions of the scaffolds compared to day 0. The staining appeared stronger in area's where clusters of cells could be identified, indicated by the black dotted circles. However, no obvious differences were observed between the scaffolds over time and between the different scaffold compositions ($THA_{2.5}$, $THA_{2.5}$-$AC_{0.5}$, $THA_{2.5}$-AC_1). Therefore, the sGAG production was quantified by determining the percentage of sGAGs per area, presented in Fig. 3.11B. For the scaffolds with $THA_{2.5}$ and $THA_{2.5}$-$AC_{0.5}$ no significant difference was found over time. However, an increasing trend over time was observed. A significant increase in the sGAG production between day 0 and 28 was seen for the scaffolds with $THA_{2.5}$-AC_1.

Besides the histological analysis, a sGAG analysis was performed to quantify the sGAG production of the cells. The results are presented in Appendix A.8. As can be seen, no appreciable sGAG formation production occurs in the $THA_{2.5}$ and $THA_{2.5}$-AC_1 samples. A significant increase was found for the samples between day 0 and day 28 for scaffolds with $THA_{2.5}$-$AC_{0.5}$.

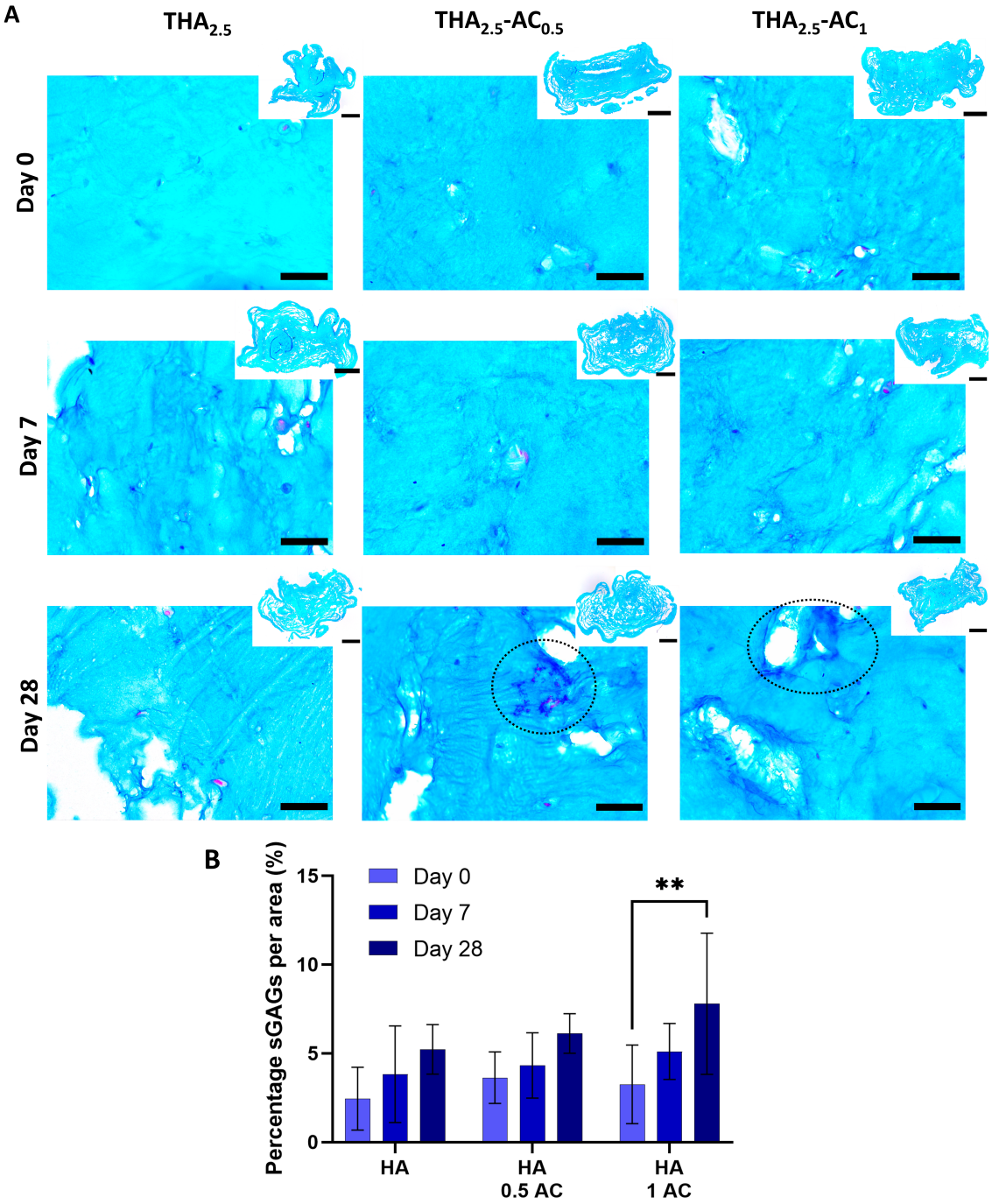

Figure 3.11: Histological images of the bioprinted scaffolds cultured after 1, 7 and 28 days and stained sGAGs (Alcian Blue). The images shown in the box on the top right, illustrate a full stained slice of the scaffold (scale bar = 1 mm), while the higher magnification images on the bottom illustrate a specific region of interest of the slice (scale bar = 100 µm).

3.7.2. Picrosirius Red

For the collagen production, the scaffolds were stained with Picrosirius Red, presented in Fig. 3.12A. At day 0, the amount of collagen produced is expected to be zero, as with the sGAGs. For $THA_{2.5}$ scaffolds, no collagen was observed. However, it can be observed that both the $THA_{2.5}$-$AC_{0.5}$ and $THA_{2.5}$-AC_1 scaffolds contain collagen. The AC dECM mostly consists of collagen, therefore this initial amount is expected. The histological images show that the AC dECM is homogeneously distributed in the bioprinted scaffolds. At day 28, it was difficult to observe whether the cells had produced collagen over time. The quantification of the collagen production determined by the percentage of collagen per area is presented in Fig. 3.12B. No significant differences in the collagen production for all the scaffolds were observed over time.

3.7.3. Hematoxylin and Eosin

The scaffolds were stained with H&E to get an indication of the cell distribution in the samples, staining the cell nuclei dark purple and ECM pink. The At day 0, the staining shows a homogeneous cell distribution in the bioprinted scaffolds for all conditions, presented in Fig. 3.13. For the $THA_{2.5}$-$AC_{0.5}$ and $THA_{2.5}$-AC_1 scaffolds, aggregates of AC dECM are visible in the pink color. After 7 and 28 days of culture, for scaffolds including AC dECM, the formation of cell clusters was observed, indicated by the black dotted circles. The cells in $THA_{2.5}$ scaffolds were still homogeneously distributed with almost no cluster formation. Furthermore, the images show that the cell clusters are centered around the AC dECM aggregates.

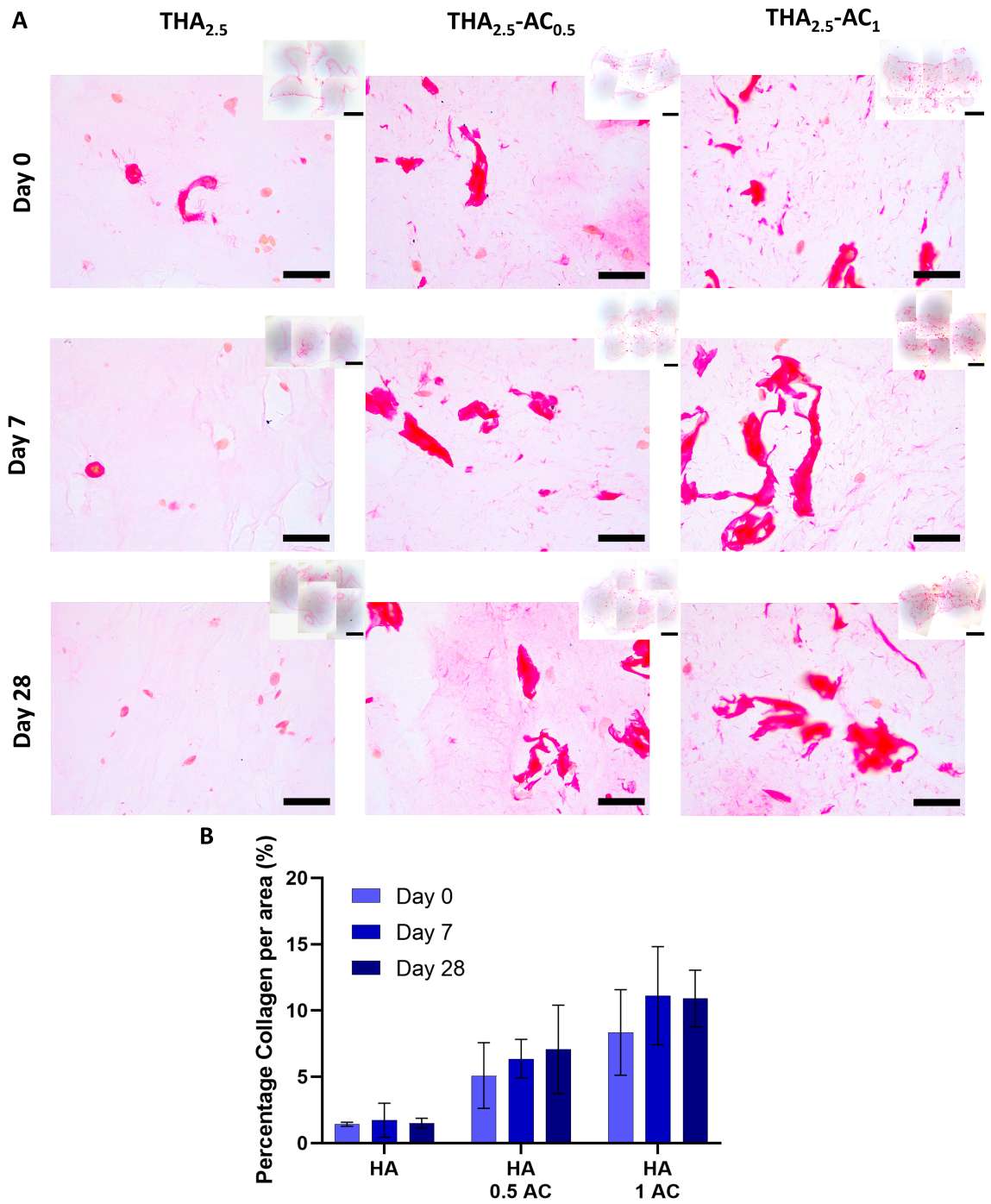

Figure 3.12: Histological images of the bioprinted scaffolds cultured after 1, 7 and 28 days and stained collagen (Picrosirius Red). The images shown in the box on the top right, illustrate a full stained slice of the scaffold (scale bar = 1 mm), while the higher magnification images on the bottom illustrate a specific region of interest of the slice (scale bar = 100 µm).

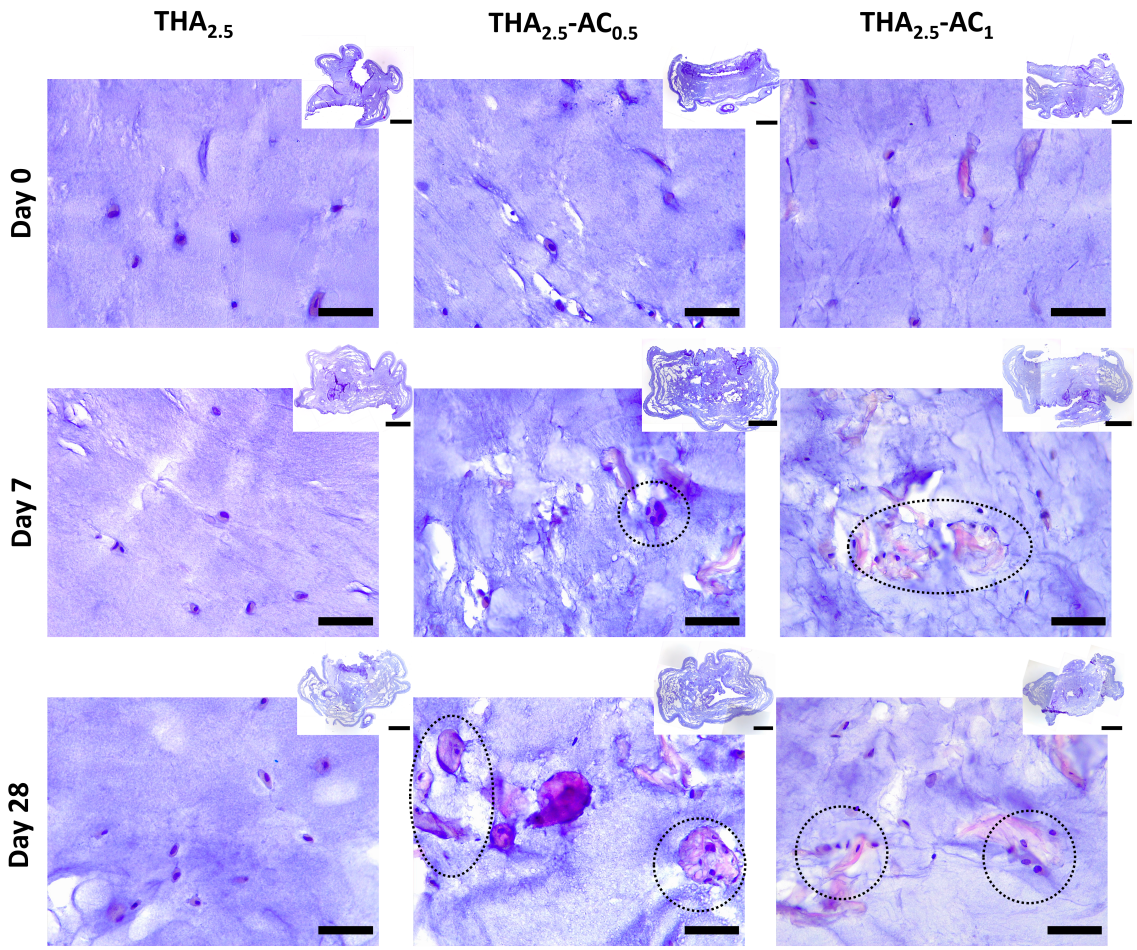

Figure 3.13: Histological images of the bioprinted scaffolds cultured after 1, 7 and 28 days and stained cell nuclei (H&E). The images shown in the box on the top right, illustrate a full stained slice of the scaffold (scale bar = 1 mm), while the higher magnification images on the bottom illustrate a specific region of interest of the slice (scale bar = 100 µm).

4

Discussion

In clinical medicine, the engineering of scaffolds with complex and hierarchical structures, is of great interest. This is particular interesting for tissues such as articular cartilage, which consists of multiple layers with differences in cell density, matrix composition, and mechanical properties. 3D bioprinting is a promising method to achieve the recapitulation of such complex tissues. However, only a small numbers of bioinks have the required properties for printability and provide a suitable environment for the cells to engineer a functional cartilage tissue. This limits the prospects of bioprinting for tissue repair, as cells are sensitive to their surroundings. To address this, we developed a cartilage specific bioink combining THA and AC dECM, that was both printable and provided cell-hydrogel interactions.

The first phase in this thesis was to identify a printable ink composition for $THA_{2.5}$. The printability of the ink is depended on the amount of enzymatic pre-crosslinking, regulated by the concentration H_2O_2. The rheological characterization showed that all inks had shear thinning behavior, which is important property for ink extrusion. Moreover, THA inks with 0.25 mM and 0.3 mM H_2O_2 showed the presence of yield stress and a recovery above 80%. However, THA with 0.1 mM H_2O_2 had almost no yield stress and only a recovery 20.8%. This difference was also observed in the printability images, where the THA ink with 0.1 mM H_2O_2 had a low shape fidelity after printing. Although, a concentration of 0.3 mM H_2 created a stiff network, it resulted in a granular printing texture. THA with 0.25 mM H_2O_2 created an ink that could be extruded and retain its shape. Hence, we decided to use this particular H_2O_2 concentration throughout the rest of the study. Next, the printability of $THA_{2.5}$ with a varying concentration of AC dECM (0.0%, 0.5% and 1.0%) was tested. The $THA_{2.5}$-$AC_{0\text{-}1}$ inks with 0.25 mM H_2O_2 all showed to have yield stress, shear thinning behavior, and recovery. Different to the $THA_{2.5}$ ink, we observed an increase in the viscosity and a decrease in the G', when AC dECM was added to the ink. Kest et al. observed similar results. Here, the viscosity of alginate/gellan bioink increased and the G' decreased, due to the addition of AC dECM [26]. This observation suggests that the presence of AC dECM may hinder crosslinking. However, it does results in a denser polymer network due to the entanglements of the AC dECM in the THA network [26, 29].

To further relate the rheology to printability of the inks, the damping factor was calculated and linked to extrusion and printability measurements. For the ink in this study, a damping

factor between 0.056-0.140 resulted in the best printability; a good balance between viscous flow and elasticity. A decrease or increase in the H_2O_2 concentration resulted in damping factor values outside this range and an ink too liquid or granular to be printed. The damping factor was chosen as a printability measurement because it only takes a few seconds to measure and is less prone to bias [29]. Moreover, when a printable damping factor range is determined, the printability of an ink could be predicted performing only rheology measurements. Therefore, it is a useful parameter for quick ink screening and can easily be compared to other papers. However, other papers reported a damping factors between 0.4-0.6 for a THA ink and 0.25-0.45 for gelatin-alginate ink for high shape fidelity [17, 18, 30]. The printable damping factor range of these bioinks is significantly different than the values found in this study, making it difficult to compare the inks. Based on these findings, it appears that the damping factor for a printable ink formulation is unique to each bioink. There are currently no standardized methods for determining a material's printability, and the development of new bioinks depends on time-consuming trial-and-error of different material formulations [11, 31]. A standard model that connects rheological and printing parameters to printability to compare results between laboratories, could aid in the development of future bioinks [29].

After the optimization of the ink composition and scaffold behavior, cells were embedded in the bioink. According to the literature, cell encapsulation may have an impact on the ink composition, depending on the bioink and crosslinking mechanism. For example, a pentanoate-functionalized HA bioink, adding cell concentrations up to 9 x 10^6 cells/ml had minimal impact on the viscosity and yield stress [11]. On the contrary, other studies found a decreasing viscosity when 2.5 x 10^6 cells/ml and 2 x 10^6 cells/ml were added to the bioink [32, 33]. Moreover, cells can interfere with the crosslinking procedure, by being a barrier between different regions of the bioink and reacting groups. This was observed for HA-based bioink with 25 x 10^6 cells/ml. Here the crosslinking time was comparable to the ink without cells. Further increase of the cell density resulted in an increased crosslinking time [34]. For a tyramine-modified HA bioink, the addition of 2.5 or 5 x 10^6 cells/ml resulted in a liquid, unprintable ink [17]. The cells most likely interfered with the crosslinking mechanism.

To avoid the cells affecting the bioink pre-crosslinking, we incorporated the cells into the bioink after enzymatic crosslinking. However, cells still occupy a certain volume within the bioink, depending on their concentration and size. High cell densities could be considered a colloidal system, by displaying shear thinning behavior and even printability without the addition of biomaterials [35–37]. Therefore, mixing cells into a bioink could turn the it into a composite material. Hence, the cells can influence the viscoelastic properties of the ink [38]. In this study, we observed that, due to the addition of cells, the ink became more sticky and liquid. Even though the cells affected the bioink's viscoelastic properties, it was still printable.

When the inks were mixed with the hMSCs, PBS was replaced by expansion medium to improve cell viability. Similar to the addition of the cells, incorporation of expansion medium altered the viscoelastic properties of the bioinks. Compared to the inks prepared with PBS, expansion medium reduced the viscosity of the inks after pre-crosslinking with 0.25

mM H_2O_2 for 60'. The inks became to sticky and liquid to be printed. To obtain a printable bioink, the H_2O_2 concentration was increased from 0.25 mM to 0.3 mM. The pre-crosslinking of THA with H_2O_2 was most likely influenced by presence of FBS serum in the expansion medium. FBS has a diverse composition (it includes enzymes) and may have peroxidase activity. Therefore it can react with the H_2O_2. As a result, the concentration of H_2O_2 was increased to guarantee enough for pre-crosslinking.

In this thesis, a dual crosslinking hydrogel is used. First enzymatic pre-crosslinking performed to ensure printability and after printing photo-crosslinking is executed in the presence of EO to ensure shape fidelity of the printed scaffold. Most photo-crosslinked bioinks are crosslinked in the presence of UV-light exposure and Irgacure 2959 as photo-initiator [11, 32, 39–41]. However, for these photo-crosslinking systems it is shown that UV-light can cause damage to cells, directly through interaction with the cell membranes, proteins and DNA or indirectly due to generation of reactive oxygen species (ROS) [42]. Because of the potential for cell damage, a green-light crosslinking system was devised, which uses visible light rather than UV radiation. To utilize this particular type of crosslinking, a unique visible light photo-initiator, EO, was added to the bioink. A disadvantage of EO is that it has a concentration dependent cytotoxic effect, independent of the light exposure [17, 43, 44]. For the inks in this research, a concentration of 0.01% w/v EO (0.15mM) was used to enable photo-crosslinking. This EO concentration is higher compared to other studies that use cell-laden hydrogel with visible light crosslinking [44–46]. However, two different studies showed high cell viability for similar or higher concentrations of EO [17, 47].

The bioprinting test, where $THA_{2.5}$ bioink was dissolved in PBS, showed that the cells were dying after 24 hours. The first possible explanation for the reduced cell viability is the cytotoxic effect of EO. Similar findings were reported in a different study that combined EO and PBS for bioprinting. Here, the cell viability decreased from 60% at 10' after printing to 0% after 60' [17]. It was suggested that, due to the lack of proteins that help maintain intracellular homeostasis and the experience of cellular stress, EO had the chance to penetrate the cell. In our experiments, EO was reconstituted in dimethyl sulfoxide (DMSO), which might have facilitated the internalization of EO, since DMSO can interact with the plasma membrane, allowing pore formation [48]. To reduce the membrane penetration and therefore toxic impact of EO, expansion medium with FBS serum was incorporated into the bioink instead of PBS. The cell viability test, for $THA_{2.5}$ and $THA_{2.5}$-AC_1 samples without printing, showed a significant improvement in cell viability.

For the bioprinting cartilage specific bioinks, all bioink combinations were successfully printed into scaffolds with viable cells and cultured for 28 days. The cell viability was only 35%-55% after 28 days, which is significantly lower than during the cell viability test without printing. This suggests that something other than EO was influencing the cell viability in the printing process. After printing, the scaffolds were photo-crosslinked for 10'. During this process the samples are subjected to air flow and some drying is visible. A possible explanation for the cell death could be that the samples dehydrate during this process causing a local increase of EO on the surface of the scaffolds, which has been shown to have negative effects on cell viability [43]. However, this difference was not seen in ordinary L/D measurements since the Leica microscope could only travel up to 1 mm into the scaffold,

therefore just measuring the outsides of the designed scaffold. A difference in the cell viability between the middle (where moisture still remains) and the outsides of the scaffolds was observed, by cutting the sample in half. The cell viability in the middle of the samples was significantly higher, 83.7%, compared to the outsides of the samples, 48.1%. Papers with similar or higher EO concentrations, that also performed photo-crosslinking, had a laser following the nozzle during printing or crosslinking samples in molds for 5 minutes, reducing the risk of dehydration. [17, 47].

Furthermore, a difference in cell morphology was observed for the hMSCs embedded in $THA_{2.5}$-$AC_{0.5}$ and $THA_{2.5}$-AC_1 scaffolds. These cells had a more elongated shape compared to the cells embedded in $THA_{2.5}$ scaffolds, which had a round cell morphology. This change in shape is caused by the cellular attachment to the hydrogel matrix. Within the hydrogel, the availability of binding sites has a substantial impact on cell behavior and morphology [49]. Cells have a more spread morphology when embedded in a hydrogel that facilitates binding sites. However, cells incorporated in hydrogels that do not facilitate these binding sites tend to have a more round morphology [49]. The addition of AC dECM to the bioink enhanced the cell adhesion to the matrix, increasing the amount of binding sites. This is consistent with previous reports, where AC dECM has been incorporated into bioink [27, 50].

In addition to the L/D assay, the metabolic activity of scaffolds was measured with a PrestoBlue assay. PrestoBlue is a resazurin based staining, that has a blue color in its oxidized form and becomes a red fluorescent dye, resorufin, when it is reduced [51, 52]. Resazurin is reduced to resorufin in cellular respiration pathways by which the cells use oxygen to help them convert glucose into energy [52]. The reduction of resazurin is correlated to the oxygen consumption of the cells [53, 54]. The PrestoBlue assay indicated that the metabolic activity for all scaffolds increased from day 1 to day 7, demonstrating that cells are active. However, after 28 days the metabolic activity significantly decreased compared to day 7. It has been shown that the cell-derived oxygen consumption is reduced during chondrogenic differentiation of hMSCs [55, 56]. Therefore, a possible explanation for the decrease in metabolic activity is that the hMSCs are differentiating into chondrocytes.

For our bioprinting process, a dual crosslinking system was implemented. The bioinks were first enzymatically pre-crosslinked to enable printing. After printing the bioprinted scaffolds were photo-crosslinkined to ensure stability. The combination of both crosslinking methods led to the creation of a network that defines the final stiffness and swelling behavior of the scaffold. In general, a high crosslinking density results in a high stiffness and low swelling ratio [57]. From day 1 to 7, the swelling and compression modulus remained constant for all scaffolds. After 28 days in culture, the swelling was significantly higher and the compression modulus lower compared to day 7, for all scaffolds. The degradation of the network may be caused by the presence of hyaluronidase produced by the cells [49, 58]. The digestion of the THA matrix may allow the cells to produce their own cellular matrix components, reorganising their surroundings and producing a new matrix [49]. The THA network may also be degraded via oxidation, by the production of ROS as a consequence of aerobic respiration [58]. THA chain cleavage can be caused by species such as superoxide anions, hydroxyl radicals, and hypochloride. However, the second sug-

gestion is less likely because it has been shown that during chrondrogenic differentiation cells have less oxygen consumption [55, 56].

To evaluate the cell distribution in the scaffolds and to reveal the production of ECM components such as sGAGs and collagen over time, histological analysis was performed. The quantification of the Alcian Blue staining showed a significant increase in the sGAG production over time for the $THA_{2.5}$-AC_1 scaffolds. A slight increase in collagen production was observed, however no significant difference was quantified for any of the conditions. Overall, a small amount of sGAGs and collagen was produced during the course of the experiment (from day 0 to day 28). The low sGAGs and collagen deposition could caused by the low cell density in the scaffold or by the inability of the cells to secrete their own matrix into the dense hydrogel surrounding. According to previous findings, cell-cell contact plays an important role in chondrogenic differentiation [59]. An increase in the cell cluster size showed a higher collagen production. Hence, it was concluded that the extent of the cell differentiation increases with the amount cell-cell contact. Maher et al. seeded 30 x 10^6 and 60 x 10^6 hMSCs/ml in a nanofibrous hydrogel to promote chondrogenic differentiation and ECM production for cartilage repair. Their paper reported that hydrogels seeded with a high cell density exhibited abundant matrix generation [60]. Similar, Erickson et al. embedded 20 x 10^6 and 60 x 10^6 hMSCs/ml in a HA hydrogel, where higher cell seeding densities increased the production of sGAGs [61]. In fact, in the histology analysis of our study, the staining appeared stronger in area's where clusters of cells could be identified.

To visualize the production of sGAGs over time, the scaffolds were stained with Alcian Blue. Alcian Blue can be prepared at pH 1, to stain specifically sGAGs [62]. THA is not a sGAG, but still the samples at day 0 were stained blue, that made the identification of small changes in sGAG production more challenging. Other papers performing histology on HA-based scaffold mostly used safranin-O for staining sGAGs [39–41, 63, 64]. This dye similarly stains sGAGs but is pH insensitive, which could result in reduced THA background staining in the scaffold. [65].

Another finding from the histology images is that the collagen, from the AC dECM, appeared as aggregates within the THA network. Since the AC dECM provides cellular attachment, more collagenous material could be beneficial for cell-matrix interaction. A more homogeneous solubilisation leading to fewer collagenous clusters, could be beneficial as well. The L/D images showed that scaffolds with $THA_{2.5}$ had individual cells evenly spread throughout the sample. However, in $THA_{2.5}$-$AC_{0.5}$ and $THA_{2.5}$-AC_1 scaffolds there was more cell cluster formation. This behavior was also observed in the H&E images, where cell clusters appeared to be more centered around the collagen aggregates. To obtain a more homogeneous distribution of the cells, the AC dECM solubilisation could be improved. For the bioink preparation, THA and AC dECM were solubilized in expansion medium, using two connecting syringes for the initial mixing and subsequently kept over night under rotation. The mixing period for this bioink could be expanded to 24 hours. Another option is to dissolve the AC dECM first and to add the THA particles to the ink the next day.

For this thesis, the traditional paraffin method was used to make histology sections. In this technique, the fixed scaffolds were first dehydrated and then embedded in wax. These

two steps are performed to harden the tissue, which makes it easier to section the samples. After sectioning, the samples were stained and imaged. However, hydrogels are sensitive to normal tissue histology methods due to their water-rich and polymeric composition. Even though we tried to optimize the histology process for THA and AC dECM hydrogels, the dehydration and wax-embedding step still resulted in shrinking and deformation of the sample. This caused the sample to tear and fold during the sectioning process. This problem is also perceived in other studies using the paraffin method for hydrogel histology [66, 67]. Another histological technique used for hydrogels and scaffolds is cryosectioning. Here, the hydrogel is left in embedding medium and frozen before sectioning, eliminating the problem of shrinkage [68].

5

Conclusion and Future Research

In this thesis, we developed a cartilage specific bioink with THA and AC dECM for 3D bioprinting. This study aimed to create a bioink with good printability and was capable of providing a microenvironment beneficial for the growth of 3D structured tissue. Using rheology and printability measurements, we observed that the addition of AC dECM caused an increase in ink viscosity, yield stress and damping factor, but still provided a printable composition. For bioprinting conditions, the incorporation of expansion medium into the bioink composition revealed itself as an important variable for improving the viability of the hMSCs in the bioink. The THA-AC dECM bioinks have been successfully bioprinted into stable scaffolds with viable cells. For the bioprinted scaffolds, it was observed that the addition of AC dECM enhanced the hMSC adhesion to the matrix. These cells had a spread cell morphology compared to cells embedded in THA scaffolds, which displayed a round cell morphology. Moreover, a higher production of sGAGs over time was observed for scaffolds with AC dECM.

Although in this research a printable THA-AC dECM bioink was created and successfully printed into viable scaffolds, there were also some limitations and prospects for future research. To determine the optimal bioink composition for bioprinting and it's corresponding printing settings, rheology and printing tests were performed. The inks for these measurements, were prepared with PBS and without hMSCs. For bioprinting with hMSCs, PBS was replaced with expansion medium to improve cell viability, causing a change in the bioink's viscoelastic properties. Moreover, the incorporation of the cells into the bioink changed it's properties by becoming more liquid. Therefore, for future study, the bioink composition and printing settings, should be optimized with the inclusion of expansion media and cells. Moreover, the influence of different cell concentrations on the bioink composition could be tested using rheological measurements.

In addition, the cell viability could be improved by considering a different photo-initiator, since EO has a toxic effect on the cells. For THA hydrogels, other photo-initiators have been used for visible light crosslinking, such as rose bengal (RB) and Riboflavin (RB) [47, 69]. The cell viability could be further improved by preventing the samples from drying during the printing process, considering that sample dehydration may have caused a local increase in EO on the outside of the scaffolds. The effect of possible dehydration can not be

investigated by comparing the cell viability of printed scaffolds with and without photo-crosslinking, because without the second crosslinking, the scaffolds are not stable enough to be placed in medium without dissolving. Instead, by generating a more humid environment, the printing setup could be improved. Moreover, printing smaller batches of scaffolds (two to four) would minimize the air exposure time, however, it will increase the overall printing time. It can also be considered to perform photo-crosslinking with a laser that follows the printing nozzle [17, 47].

From the L/D images it was observed that the addition of AC dECM to the bioink resulted in a spread morphology for the cells. It might be interesting to perform actin staining, which provides better visualisation of the cell spreading by staining the actin filament in the cytoskeleton and could be used for further quantification. For this thesis, an attempt has already been made to use actin staining. However, the protocol was not yet optimized and some background staining was still present. Another interesting topic for future work is to explore the use of higher cell densities for this THA-AC dECM bioink. Other studies showed that higher cell densities improved chondrogenic differentiation and the ECM productions, due to an increase in cell-cell interactions. Moreover, for the histology analysis of our study, the Alcian Blue staining appeared stronger in area's where clusters of cells could be identified.

Finally, the histological process could be improved to provide clearer visualization of sGAGs and collagen production. The blue background staining of the Alcian Blue makes it challenging to see the sGAG production over time. For future work, it may be interesting to stain with Safranin-O staining instead of the Alcian Blue staining, to validate the results with other papers performing histological analysis on HA-based scaffolds. Moreover, to reduce the sample shrinkage, folding and tearing during the dehydration and sectioning process of histology, cryosectioning might be an option to improve the shape preservation of the scaffolds.

A potential concept to create a scaffold with a more similar structure to native articular cartilage, is the fabrication of a multilayered construct. AC consists of four distinct zones, each having its own composition, cell density, organization and ECM components, resulting in different mechanical properties per zone [1]. A single scaffold could implement a biphasic or triphasic designs to mimic the different mechanical properties of the zones. Or a zonal cartilage scaffold may be created by using different cell densities in different layers.

Bioprinting is a emerging new field with the potential to create engineered tissues with biomimetic properties similar to those of native tissues. In this study, THA-AC dECM bioinks have been successfully bioprinted to create a scaffold for articular cartilage tissue engineering. As with all new techniques, the development of this cartilage specific bioink had some challenges and limitations that need to be addressed for further improvement. However, despite the limitations of this research, the effect of AC on the cells was evident as the cells were more spread and a higher percentage of sGAGs was observed. Therefore warranting further research into the development of bioinks with tissue-specific inductive properties.

Bibliography

[1] A. J. Sophia Fox, A. Bedi, and S. A. Rodeo, "The basic science of articular cartilage: Structure, composition, and function," *Sports Health*, vol. 1, no. 6, pp. 461–468, 11 2009.

[2] C. T. Hung and V. C. Mow, "Biomechanics of Articular Cartilage," in *Basic Biomechanics of the Musculoskeletal System*, 3rd ed., M. Nordin and V. H. Frankel, Eds. Philadelphia: Lippincott Williams & Wilkins, 2001, ch. 3, pp. 60–101.

[3] I. Martin, S. Miot, A. Barbero, M. Jakob, and D. Wendt, "Osteochondral tissue engineering," *Journal of Biomechanics*, vol. 40, no. 4, pp. 750–765, 1 2007.

[4] E. Hunziker, "Articular cartilage repair: basic science and clinical progress. A review of the current status and prospects," *Osteoarthritis and Cartilage*, vol. 10, no. 6, pp. 432–463, 6 2002.

[5] L. Roseti, C. Cavallo, G. Desando, V. Parisi, M. Petretta, I. Bartolotti, and B. Grigolo, "Three-dimensional bioprinting of cartilage by the use of stem cells: A strategy to improve regeneration," 9 2018.

[6] J. H. Galarraga, M. Y. Kwon, and J. A. Burdick, "3D bioprinting via an in situ crosslinking technique towards engineering cartilage tissue," *Scientific Reports*, vol. 9, no. 1, pp. 1–12, 12 2019.

[7] P. S. Gungor-Ozkerim, I. Inci, Y. S. Zhang, A. Khademhosseini, and M. R. Dokmeci, "Bioinks for 3D bioprinting: An overview," pp. 915–946, 5 2018.

[8] J. Groll, J. A. Burdick, D. W. Cho, B. Derby, M. Gelinsky, S. C. Heilshorn, T. Jüngst, J. Malda, V. A. Mironov, K. Nakayama, A. Ovsianikov, W. Sun, S. Takeuchi, J. J. Yoo, and T. B. Woodfield, "A definition of bioinks and their distinction from biomaterial inks," p. 013001, 1 2019.

[9] M. E. Cooke and D. H. Rosenzweig, "The rheology of direct and suspended extrusion bioprinting," p. 11502, 3 2021.

[10] S. Boularaoui, G. Al Hussein, K. A. Khan, N. Christoforou, and C. Stefanini, "An overview of extrusion-based bioprinting with a focus on induced shear stress and its effect on cell viability," p. e00093, 12 2020.

[11] E. A. Kiyotake, A. W. Douglas, E. E. Thomas, S. L. Nimmo, and M. S. Detamore, "Development and quantitative characterization of the precursor rheology of hyaluronic acid hydrogels for bioprinting," *Acta Biomaterialia*, vol. 95, pp. 176–187, 9 2019.

[12] K. J. Wolf and S. Kumar, "Hyaluronic Acid: Incorporating the Bio into the Material," pp. 3753–3765, 8 2019.

[13] R. V. Iozzo and L. Schaefer, "Proteoglycan form and function: A comprehensive nomenclature of proteoglycans," pp. 11–55, 3 2015.

[14] M. T. Poldervaart, B. Goversen, M. de Ruijter, A. Abbadessa, F. P. W. Melchels, F. C. Öner, W. J. A. Dhert, T. Vermonden, and J. Alblas, "3D bioprinting of methacrylated hyaluronic acid (MeHA) hydrogel with intrinsic osteogenicity," *PLOS ONE*, vol. 12, no. 6, p. e0177628, 6 2017.

[15] C. B. Highley, C. B. Rodell, and J. A. Burdick, "Direct 3D Printing of Shear-Thinning Hydrogels into Self-Healing Hydrogels," *Advanced Materials*, vol. 27, no. 34, pp. 5075–5079, 9 2015.

[16] L. Ouyang, C. B. Highley, C. B. Rodell, W. Sun, and J. A. Burdick, "3D Printing of Shear-Thinning Hyaluronic Acid Hydrogels with Secondary Cross-Linking," *ACS Biomaterials Science and Engineering*, vol. 2, no. 10, pp. 1743–1751, 10 2016.

[17] D. Petta, A. R. Armiento, D. Grijpma, M. Alini, D. Eglin, and M. D'este, "3D bioprinting of a hyaluronan bioink through enzymatic-and visible light-crosslinking," *Biofabrication*, vol. 10, no. 4, 2018.

[18] D. Petta, D. W. Grijpma, M. Alini, D. Eglin, and M. D'Este, "Three-Dimensional Printing of a Tyramine Hyaluronan Derivative with Double Gelation Mechanism for Independent Tuning of Shear Thinning and Postprinting Curing," *ACS Biomaterials Science and Engineering*, vol. 4, no. 8, pp. 3088–3098, 8 2018.

[19] X. Z. Shu, K. Ghosh, Y. Liu, F. S. Palumbo, Y. Luo, R. A. Clark, and G. D. Prestwich, "Attachment and spreading of fibroblasts on an RGD peptide–modified injectable hyaluronan hydrogel," *Journal of Biomedical Materials Research Part A*, vol. 68A, no. 2, pp. 365–375, 2 2004.

[20] A. J. Vernengo, S. Grad, D. Eglin, M. Alini, and Z. Li, "Bioprinting Tissue Analogues with Decellularized Extracellular Matrix Bioink for Regeneration and Tissue Models of Cartilage and Intervertebral Discs," *Advanced Functional Materials*, vol. 30, no. 44, p. 1909044, 10 2020.

[21] J. Engel and M. Chiquet, "An Overview of Extracellular Matrix Structure and Function," in *The Extracellular Matrix: an Overview*. Springer Berlin Heidelberg, 2011, pp. 1–39.

[22] D. C. Browe, O. R. Mahon, P. J. Díaz-Payno, N. Cassidy, I. Dudurych, A. Dunne, C. T. Buckley, and D. J. Kelly, "Glyoxal cross-linking of solubilized extracellular matrix to produce highly porous, elastic, and chondro-permissive scaffolds for orthopedic tissue engineering," *Journal of Biomedical Materials Research - Part A*, vol. 107, no. 10, pp. 2222–2234, 10 2019.

[23] H. V. Almeida, Y. Liu, G. M. Cunniffe, K. J. Mulhall, A. Matsiko, C. T. Buckley, F. J. O'Brien, and D. J. Kelly, "Controlled release of transforming growth factor-β3 from cartilage-extra-cellular-matrix-derived scaffolds to promote chondrogenesis of human-joint-tissue-derived stem cells," *Acta Biomaterialia*, vol. 10, no. 10, pp. 4400–4409, 10 2014.

[24] H. V. Almeida, G. M. Cunniffe, T. Vinardell, C. T. Buckley, F. J. O'Brien, and D. J. Kelly, "Coupling Freshly Isolated CD44+ Infrapatellar Fat Pad-Derived Stromal Cells with a TGF-β3 Eluting Cartilage ECM-Derived Scaffold as a Single-Stage Strategy for Promoting Chondrogenesis," *Advanced Healthcare Materials*, vol. 4, no. 7, pp. 1043–1053, 5 2015.

[25] G. M. Cunniffe, P. J. Díaz-Payno, E. J. Sheehy, S. E. Critchley, H. V. Almeida, P. Pitacco, S. F. Carroll, O. R. Mahon, A. Dunne, T. J. Levingstone, C. J. Moran, R. T. Brady, F. J. O'Brien, P. A. Brama, and D. J. Kelly, "Tissue-specific extracellular matrix scaffolds for the regeneration of spatially complex musculoskeletal tissues," *Biomaterials*, vol. 188, pp. 63–73, 1 2019.

[26] M. Kesti, C. Eberhardt, G. Pagliccia, D. Kenkel, D. Grande, A. Boss, and M. Zenobi-Wong, "Bioprinting Complex Cartilaginous Structures with Clinically Compliant Biomaterials," *Advanced Functional Materials*, vol. 25, no. 48, pp. 7406–7417, 12 2015.

[27] W. Chen, Y. Xu, Y. Li, L. Jia, X. Mo, G. Jiang, and G. Zhou, "3D printing electrospinning fiber-reinforced decellularized extracellular matrix for cartilage regeneration," *Chemical Engineering Journal*, vol. 382, p. 122986, 2 2020.

[28] O. R. Mahon, D. C. Browe, P. J. Diaz-Payno, P. Pitacco, K. T. Cunningham, K. H. Mills, A. Dunne, and D. J. Kelly, "Extracellular matrix scaffolds derived from different musculoskeletal tissues drive distinct macrophage phenotypes and direct tissue-specific cellular differentiation," *Journal of Immunology and Regenerative Medicine*, vol. 12, p. 100041, 5 2021.

[29] A. Schwab, R. Levato, M. D'Este, S. Piluso, D. Eglin, and J. Malda, "Printability and Shape Fidelity of Bioinks in 3D Bioprinting," *Chemical Reviews*, vol. 120, no. 19, pp. 11 028–11 055, 10 2020.

[30] L. Ouyang, R. Yao, and Y. Zhao, "Optimization of gelatin-alginate composite bioink printability using rheological parameters: a systematic approach Related content Effect of bioink properties on printability and cell viability for 3D bioplotting of embryonic stem cells," 2018.

[31] J. Malda, J. Visser, F. P. Melchels, T. Jüngst, W. E. Hennink, W. J. Dhert, J. Groll, and D. W. Hutmacher, "25th anniversary article: Engineering hydrogels for biofabrication," pp. 5011–5028, 9 2013.

[32] L. Ouyang, R. Yao, Y. Zhao, and W. Sun, "Effect of bioink properties on printability and cell viability for 3D bioplotting of embryonic stem cells," *Biofabrication*, vol. 8, no. 3, p. 035020, 9 2016.

[33] T. Billiet, E. Gevaert, T. De Schryver, M. Cornelissen, and P. Dubruel, "The 3D printing of gelatin methacrylamide cell-laden tissue-engineered constructs with high cell viability," *Biomaterials*, vol. 35, no. 1, pp. 49–62, 1 2014.

[34] A. Skardal, J. Zhang, L. McCoard, X. Xu, S. Oottamasathien, and G. D. Prestwich, "Photocrosslinkable hyaluronan-gelatin hydrogels for two-step bioprinting," *Tissue Engineering - Part A*, vol. 16, no. 8, pp. 2675–2685, 8 2010.

[35] A. Lee, A. R. Hudson, D. J. Shiwarski, J. W. Tashman, T. J. Hinton, S. Yerneni, J. M. Bliley, P. G. Campbell, and A. W. Feinberg, "3D bioprinting of collagen to rebuild components of the human heart," *Science*, vol. 365, no. 6452, pp. 482–487, 8 2019.

[36] M. A. Skylar-Scott, S. G. Uzel, L. L. Nam, J. H. Ahrens, R. L. Truby, S. Damaraju, and J. A. Lewis, "Biomanufacturing of organ-specific tissues with high cellular density and embedded vascular channels," *Science Advances*, vol. 5, no. 9, p. eaaw2459, 9 2019.

[37] O. Jeon, Y. B. Lee, H. Jeong, S. J. Lee, D. Wells, and E. Alsberg, "Individual cell-only bioink and photocurable supporting medium for 3D printing and generation of engineered tissues with complex geometries," *Materials Horizons*, vol. 6, no. 8, pp. 1625–1631, 10 2019.

[38] R. Schwartz, M. Malpica, G. L. Thompson, and A. K. Miri, "Cell encapsulation in gelatin bioink impairs 3D bioprinting resolution," *Journal of the Mechanical Behavior of Biomedical Materials*, vol. 103, p. 103524, 3 2020.

[39] B. Duan, E. Kapetanovic, L. A. Hockaday, and J. T. Butcher, "Three-dimensional printed trileaflet valve conduits using biological hydrogels and human valve interstitial cells," *Acta Biomaterialia*, vol. 10, no. 5, pp. 1836–1846, 2014.

[40] V. H. Mouser, A. Abbadessa, R. Levato, W. E. Hennink, T. Vermonden, D. Gawlitta, and J. Malda, "Development of a thermosensitive HAMA-containing bio-ink for the fabrication of composite cartilage repair constructs," *Biofabrication*, vol. 9, no. 1, 3 2017.

[41] S. Stichler, T. Böck, N. Paxton, S. Bertlein, R. Levato, V. Schill, W. Smolan, J. Malda, J. Teßmar, T. Blunk, and J. Groll, "Double printing of hyaluronic acid/poly(glycidol) hybrid hydrogels with poly(epsilon-caprolactone) for MSC chondrogenesis," *Biofabrication*, vol. 9, no. 4, 11 2017.

[42] J. Dahle, E. Kvam, and T. Stokke, "Bystander effects in UV-induced genomic instability: Antioxidants inhibit delayed mutagenesis induced by ultraviolet A and B radiation," *Journal of Carcinogenesis*, vol. 4, p. 11, 8 2005.

[43] Y. Liu, Y. Chen, Y. Shi, D. Wan, J. Chen, and S. Xiao, "Adsorption of toxic dye Eosin Y from aqueous solution by clay/carbon composite derived from spent bleaching earth," *Water Environment Research*, vol. 93, no. 1, pp. 159–169, 1 2021.

[44] C. S. Bahney, T. J. Lujan, C. W. Hsu, M. Bottlang, J. L. West, and B. Johnstone, "Visible light photoinitiation of mesenchymal stem cell-laden bioresponsive hydrogels," *European Cells and Materials*, vol. 22, pp. 43–55, 2011.

[45] H. Shih and C. C. Lin, "Visible-light-mediated thiol-ene hydrogelation using eosin-Y as the only photoinitiator," *Macromolecular Rapid Communications*, vol. 34, no. 3, pp. 269–273, 2 2013.

[46] Z. Wang, R. Abdulla, B. Parker, R. Samanipour, S. Ghosh, and K. Kim, "A simple and high-resolution stereolithography-based 3D bioprinting system using visible light crosslinkable bioinks," *Biofabrication*, vol. 7, no. 4, p. 045009, 12 2015.

[47] C. Loebel, N. Broguiere, M. Alini, M. Zenobi-Wong, and D. Eglin, "Microfabrication of photo-cross-linked hyaluronan hydrogels by single- and two-photon tyramine oxidation," *Biomacromolecules*, vol. 16, no. 9, pp. 2624–2630, 9 2015.

[48] L. De Abreu Costa, M. H. F. Ottoni, M. G. Dos Santos, A. B. Meireles, V. G. De Almeida, W. De Fátima Pereira, B. A. De Avelar-Freitas, and G. E. A. Brito-Melo, "Dimethyl sulfoxide (DMSO) decreases cell proliferation and TNF-α, IFN-, and IL-2 cytokines production in cultures of peripheral blood lymphocytes," *Molecules*, vol. 22, no. 11, p. 1789, 11 2017.

[49] M. Ahearne, "Introduction to cell–hydrogel mechanosensing," *Interface Focus*, vol. 4, no. 2, p. 20130038, 4 2014.

[50] F. Pati, J. Jang, D. H. Ha, S. Won Kim, J. W. Rhie, J. H. Shim, D. H. Kim, and D. W. Cho, "Printing three-dimensional tissue analogues with decellularized extracellular matrix bioink," *Nature Communications*, vol. 5, no. 1, pp. 1–11, 6 2014.

[51] M. Xu, D. J. McCanna, and J. G. Sivak, "Use of the viability reagent PrestoBlue in comparison with alamarBlue and MTT to assess the viability of human corneal epithelial cells," *Journal of Pharmacological and Toxicological Methods*, vol. 71, pp. 1–7, 1 2015.

[52] O. Braissant, M. Astasov-Frauenhoffer, T. Waltimo, and G. Bonkat, "A Review of Methods to Determine Viability, Vitality, and Metabolic Rates in Microbiology," p. 2726, 11 2020.

[53] R. González-Pinzón, R. Haggerty, and D. D. Myrold, "Measuring aerobic respiration in stream ecosystems using the resazurin-resorufin system," *J. Geophys. Res*, vol. 117, pp. 0–06.

[54] D. Liu, "Resazurin Reduction Method for Activated Sludge Process Control," *Environmental Science and Technology*, vol. 17, no. 7, pp. 407–411, 1983.

[55] S. F. Carroll, C. T. Buckley, and D. J. Kelly, "Measuring and Modeling Oxygen Transport and Consumption in 3D Hydrogels Containing Chondrocytes and Stem Cells of Different Tissue Origins," *Frontiers in Bioengineering and Biotechnology*, vol. 9, p. 328, 5 2021.

[56] G. Pattappa, H. K. Heywood, J. D. d. Bruijn, and D. A. Lee, "The metabolism of human mesenchymal stem cells during proliferation and differentiation," *Journal of Cellular Physiology*, vol. 226, no. 10, pp. 2562–2570, 10 2011.

[57] K. I. Hoshino, T. Nakajima, T. Matsuda, T. Sakai, and J. P. Gong, "Network elasticity of a model hydrogel as a function of swelling ratio: From shrinking to extreme swelling states," *Soft Matter*, vol. 14, no. 47, pp. 9693–9701, 12 2018.

[58] A. Fakhari and C. Berkland, "Applications and emerging trends of hyaluronic acid in tissue engineering, as a dermal filler and in osteoarthritis treatment," *Acta Biomaterialia*, vol. 9, no. 7, pp. 7081–7092, 7 2013.

[59] B. Cao, Z. Li, R. Peng, and J. Ding, "Effects of cell–cell contact and oxygen tension on chondrogenic differentiation of stem cells," *Biomaterials*, vol. 64, pp. 21–32, 9 2015.

[60] S. A. Maher, R. L. Mauck, L. Rackwitz, and R. S. Tuan, "A nanofibrous cell-seeded hydrogel promotes integration in a cartilage gap model," *Journal of Tissue Engineering and Regenerative Medicine*, vol. 4, no. 1, pp. 25–29, 1 2010.

[61] I. E. Erickson, S. R. Kestle, K. H. Zellars, M. J. Farrell, M. Kim, J. A. Burdick, and R. L. Mauck, "High mesenchymal stem cell seeding densities in hyaluronic acid hydrogels produce engineered cartilage with native tissue properties," *Acta Biomaterialia*, vol. 8, no. 8, pp. 3027–3034, 8 2012.

[62] S. A. Alexander and R. B. Donoff, "A Modification of the Alcian Blue Method for Staining Hyaluronic Acid Substances in Tissue Sections," *Journal of Histotechnology*, vol. 3, no. 2, pp. 41–44, 1980.

[63] A. Abbadessa, V. H. Mouser, M. M. Blokzijl, D. Gawlitta, W. J. Dhert, W. E. Hennink, J. Malda, and T. Vermonden, "A Synthetic Thermosensitive Hydrogel for Cartilage Bioprinting and Its Biofunctionalization with Polysaccharides," *Biomacromolecules*, vol. 17, no. 6, pp. 2137–2147, 6 2016.

[64] A. Schwab, C. Helary, G. Richards, M. Alini, D. Eglin, and M. D'Este, "Tissue mimetic hyaluronan bio-ink containing oriented collagen fibers to modulate hMSC spreading and differentiation," *bioRxiv*, p. 2020.02.26.966564, 4 2020.

[65] A. Wall and T. Board, "Chemical basis for the histological use of safranin o in the study of articular cartilage," in *Classic Papers in Orthopaedics*. Springer-Verlag London Ltd, 1 2014, pp. 433–435.

[66] R. James, L. Jenkins, S. E. Ellis, and K. J. Burg, "Histological processing of hydrogel scaffolds for tissue-engineering applications," *Journal of Histotechnology*, vol. 27, no. 2, pp. 133–139, 2004.

[67] A. B. Loebsack, C. R. Halberstadt, W. D. Holder, C. R. Culberson, R. J. Beiler, K. G. Greene, W. D. Roland, and K. J. L. Burg, "The Development of an Embedding Technique for Polylactide Sponges," Tech. Rep., 1999.

[68] J. L. Ruan, N. L. Tulloch, V. Muskheli, E. E. Genova, P. D. Mariner, K. S. Anseth, and C. E. Murry, "An improved cryosection method for polyethylene glycol hydrogels used in tissue engineering," *Tissue Engineering - Part C: Methods*, vol. 19, no. 10, pp. 794–801, 10 2013.

[69] B. M. Hong, S. A. Park, and W. H. Park, "Effect of photoinitiator on chain degradation of hyaluronic acid," *Biomaterials Research 2019 23:1*, vol. 23, no. 1, pp. 1–8, 11 2019.

A

Appendix

A.1. Printability assessment

To optimize the printing settings (pressure, speed and nozzle size) for each ink, a printing test was performed. For two nozzle sizes (22G and 25G), the printing speed (4,5,6 and 7 mm/s) and the printable pressures (40 to 70 kPa) were varied. The structure consists of printing one layer of a meandering pattern composed of parallel strands with increasing printing speed (2 t/m 4 mm/s or 5 t/m 7 mm/s). To create the pattern, a g-code was generated in Camotics, where the parallel strands have a length of 10 mm with a distance of 3 mm (Fig. A.1).

The inks were loaded into the Bio X bioprinter and the structure was printed on a glass microscope slide (76 mm x 26 mm, Thermo Scientific). Images of the printed bioinks were captured with the Wi-Fi Digital Microscope (ROTEK, resolution 1280 x 720 pixels) directly after printing. ImageJ was used to measure the filament width of bioprinted structures. The mean of the width of 3 filaments of each formulation are used in further results.

The optimal printing were assessed by measuring the filament width of the inks. The effect of the printing speed, pressure and nozzle size can be seen in Figure A.2, A.3 and A.4. Overall, we observed that a constant pressure and an increase in the printing speed (2 to 7 mm/s), led to decrease in the filament width. Although, a lower filament width was found for the 25G nozzle compared to the 22G nozzle, the printing pressure also increase for a smaller size. An overview of the optimal printing setting for each ink are presented in Table A.1. The best filament width was obtained using a 25G nozzle, a speed of 7 mm/s and a varying pressure for each ink.

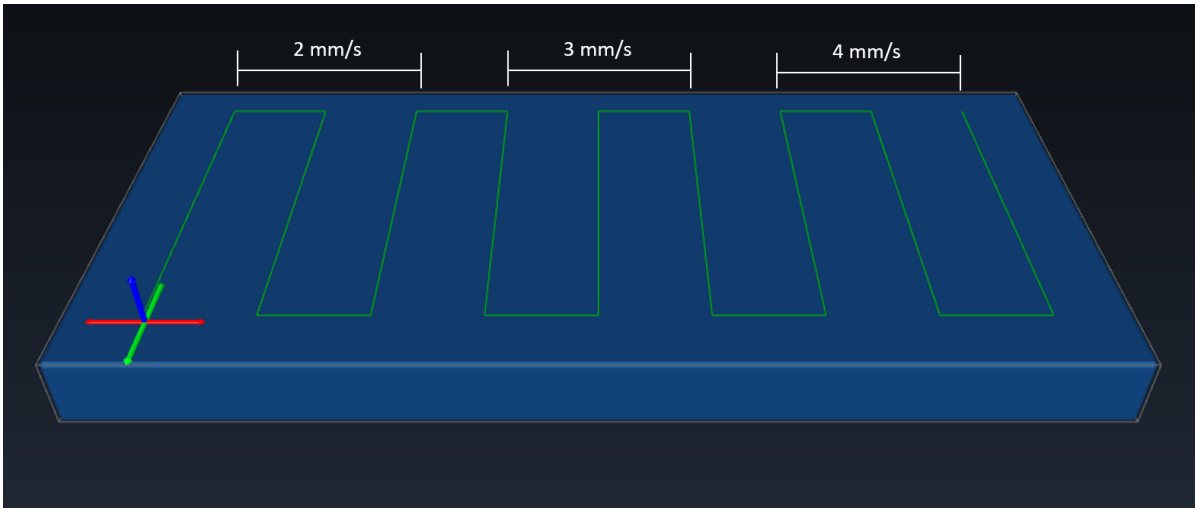

Figure A.1: Bioprinting test protocol generated in Camotics with increasing printing speed from 2 to 4 mm/s. The same design was used for increasing speeds from 5 to 7 mm/s.

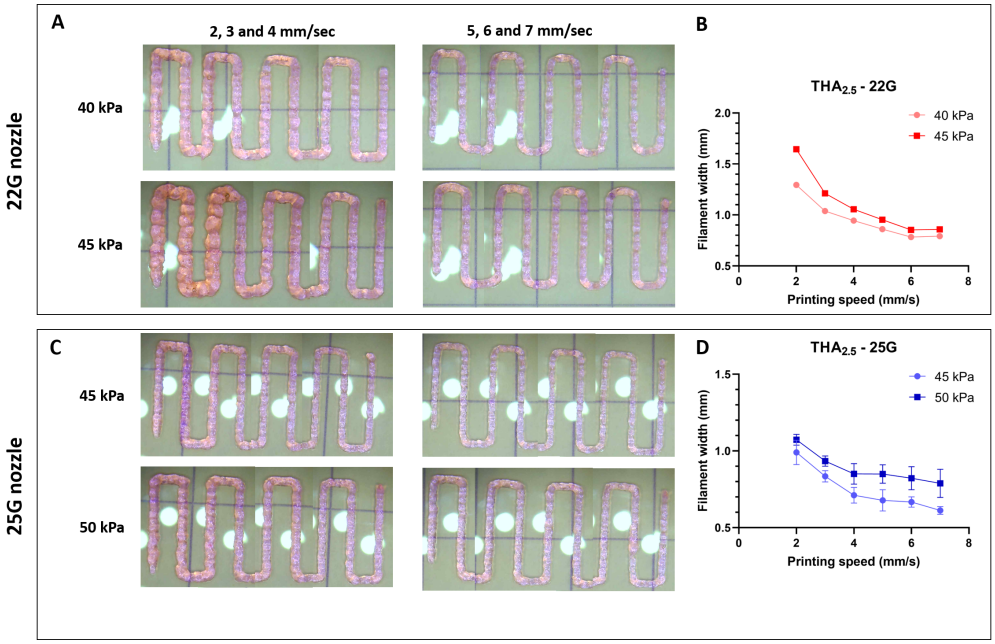

Figure A.2: Influence of the pressure, printing speed and nozzle size on the filament width for the $THA_{2.5}$ ink. A,C) Images of the printability test for the 22G and 25G nozzle. B,D) The measured filament width by varying the speed and pressure for the 22G and 25G nozzle.

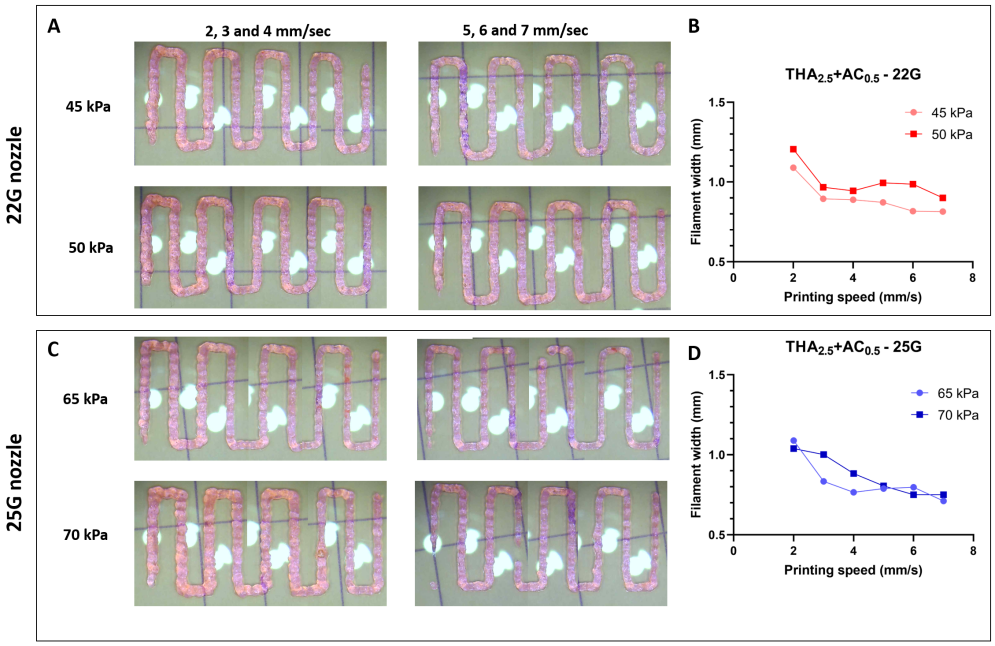

Figure A.3: Influence of the pressure, printing speed and nozzle size on the filament width for the $THA_{2.5}$-$AC_{0.5}$ ink. A,C) Images of the printability test for the 22G and 25G nozzle. B,D) The measured filament width by varying the speed and pressure for the 22G and 25G nozzle.

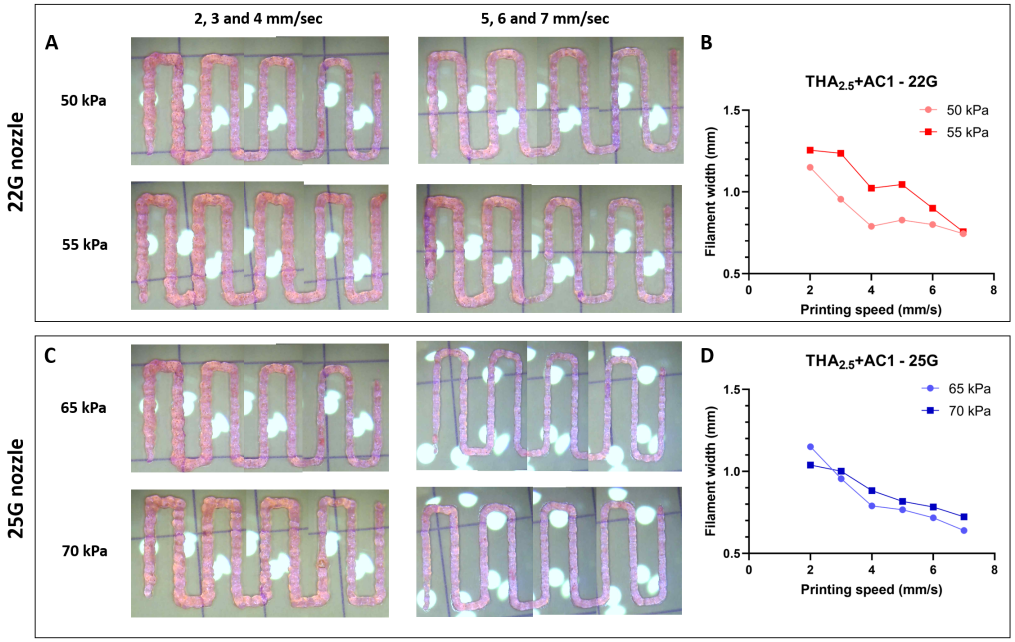

Figure A.4: Influence of the pressure, printing speed and nozzle size on the filament width for the $THA_{2.5}$-AC_1 ink. A,C) Images of the printability test for the 22G and 25G nozzle. B,D) The measured filament width by varying the speed and pressure for the 22G and 25G nozzle.

Table A.1: An overview of the optimal printing pressure and speed for each ink ($THA_{2.5}$, $THA_{2.5}$-$AC_{0.5}$, $THA_{2.5}$-AC_1) and nozzle size (22G and 25G).

Bioink	**Nozzle**	**Printing pressure**	**Printing speed**	**Filament width**
THA	22G (0.41 mm)	40 kPa	7 mm/s	0.792
	25G (0.25 mm)	45 kPa	7 mm/s	0.612
THA - 0.5% AC	22G (0.41 mm)	50 kPa	7 mm/s	0.901
	25G (0.25 mm)	65 kPa	7 mm/s	0.711
THA - 1% AC	22G (0.41 mm)	55 kPa	7 mm/s	0.765
	25G (0.25 mm)	60 kPa	7 mm/s	0.640

A.2. Scaffolds without photo-crosslinking

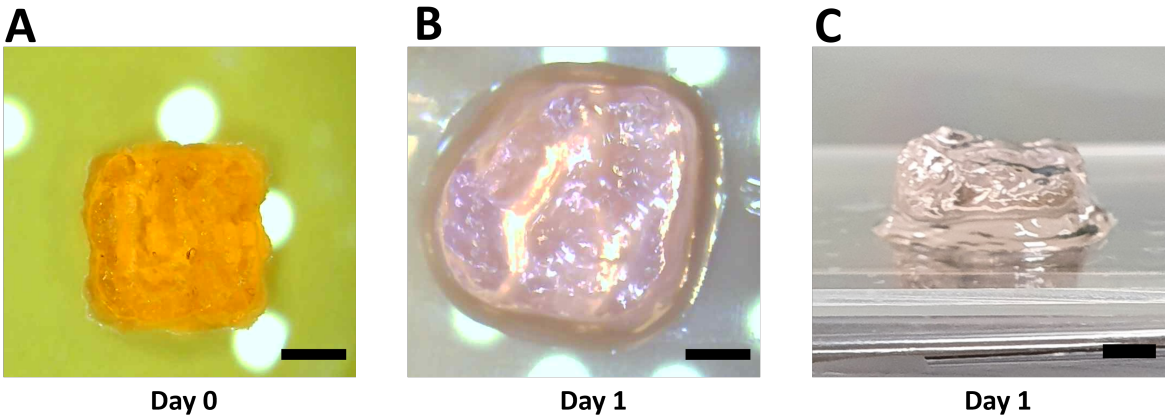

Figure A.5: Printed scaffolds without photo-crosslinking. Scale bare = 2 mm. A) Top view of scaffold immediately after printing (t=0), width = 5.5 mm. B) Top view of scaffold after 1 day in PBS, width = 7.9 mm. C) Side view of scaffold after 1 day.

A.3. L/D images day 1 of bioprinting

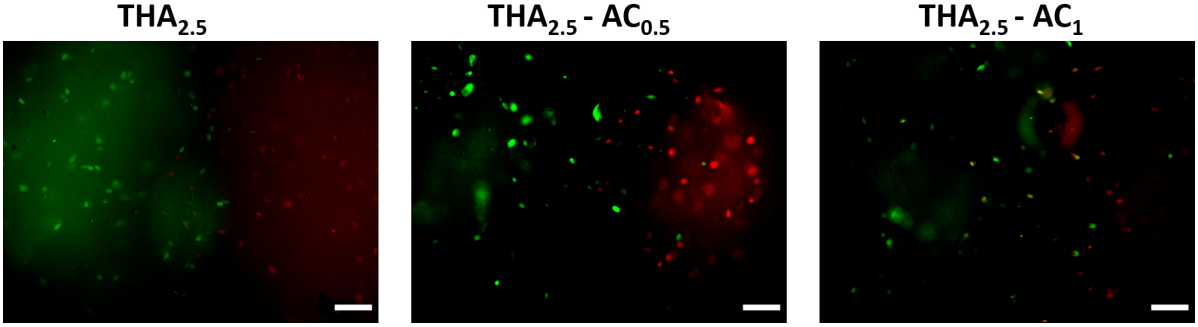

Figure A.6: L/D images of day 1 for $THA_{2.5}$, $THA_{2.5}$-$AC_{0.5}$ and $THA_{2.5}$-AC_1 and cell density of 5 x 10^6 cells/ml. Scale bar = 100 µm

A.4. Cell viability inside vs. outside scaffold

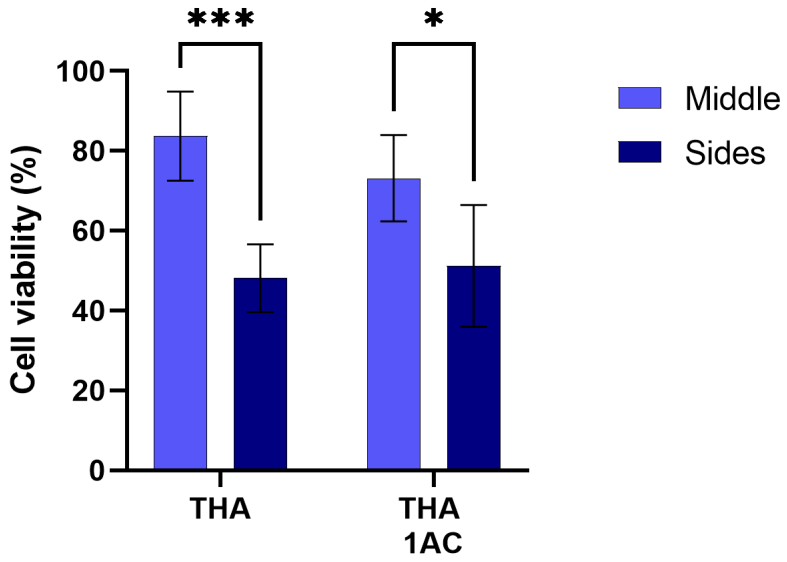

Figure A.7: Cell viability of $THA_{2.5}$ and $THA_{2.5}$-AC_1 samples obtained from L/D images of day 2. The samples have a cell density of 3 x 10^6 cells/ml.

A.5. Actin staining

Actin stains are used in living and fixed cells to study the structure and function of the cytoskeleton. The staining was performed on samples that were initially prepared to test the influence of the bioink composition on cell viability. Due to observation of the elongated shape change for the $THA_{2.5}$-AC_1 samples compared to $THA_{2.5}$ samples, it was decided to perform actin-nuclei staining on the remaining on day 10.

The samples, hMSC embedded in $THA_{2.5}$ or $THA_{2.5}$-AC_1 hydrogel, were washed 3 times with PBS and fixed overnight with 4% PFA at 4°C. The next day, the samples were again washed 3 times with PBS and the cells were permeabilized with 0.5% Triton X-100 for 20' at 4°C in the shaker. After that, the samples were washed three times with PBS, and non-specific binding was inhibited with 1% BSA in PBS for 60'. The actin filaments were stained by soaking the samples in Phalloidin (1:1000, Thermo Fisher) diluted in 1% BSA for 120' at room temperature in the shaker. Following that, the samples were incubated with 1 µg/ml Hoechst (ThermoFisher) in PBS for 15' at room temperature in the shaker, to stain the cell nuclei. The staining solution was discarded and the samples were transferred to PBS. For imaging, the scaffolds were placed on a glass slide (Menzel-Glaser Superfrost, ThermoScientific) and imaged with fluorescent microscope (ZOE fluorescent cell imager, Biorad).

The actin-nulcei staining of the $THA_{2.5}$ and $THA_{2.5}$-AC_1 samples is presented in Fig. A.8. For the $THA_{2.5}$ samples, the actin is in a round shape around the cell nuclei, while the actin for cells embedded in $THA_{2.5}$-AC_1 hydrogel is more elongated. The hMSCs embedded in $THA_{2.5}$ preserved their round shape after 10 days of culture and the cells in the $THA_{2.5}$-AC_1 hydrogel appeared to be spread. In addition, the cells seem to form cell clusters in the $THA_{2.5}$-AC_1 sample.

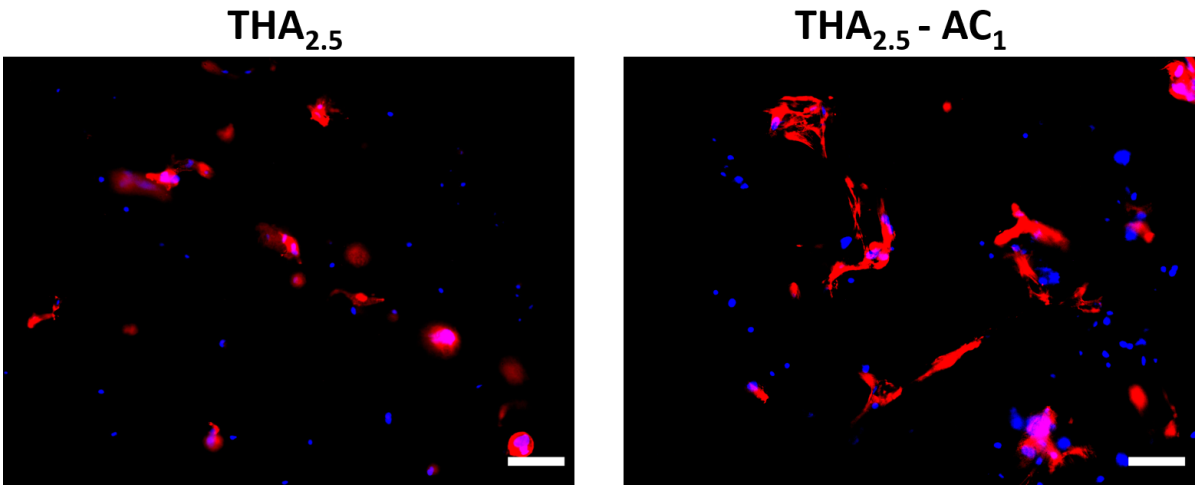

Figure A.8: Actin staining of hMSC embedded in a $THA_{2.5}$ and $THA_{2.5}$-AC_1 after 10 days in culture. Scale bar = 100 µm

A.6. Histology optimization

The standard histology procedure consists of 6 steps: fixation, dehydration, wax-embedding, slicing, staining and imaging. To assess whether the histological process was working for the printed scaffolds, first a test was performed with $THA_{2.5}$ scaffolds. After printing the scaffolds were fixed in 4% PFA and 30 mM $CaCl_2$ overnight. Next, the standard dehydration and embedding was performed, an overview of steps is presented in Table A.6. After dehydration, the scaffolds had shrunk and had not kept their shape well. Subsequently the scaffold were embedded and sectioned into slices. However, the scaffolds didn't incorporate well into the paraffin, presented in Fig. A.9A. This detachment may be caused by the interface difference, since the hydrogel scaffolds were soft and the paraffin becomes very hard.

To improve the histology process, the samples were embedded in 3% agarose after the fixation step. The goal was to reduce the sample shrinkage and to create a stiffness gradient between the hydrogel and paraffin to improve the wax embedding. In addition, we also doubled the time of dehydration step to make reduce the shrinkage of the samples. Although the long dehydration and agarose embedding improved the scaffold shrinking and embedding, it was very difficult to get the scaffold embedded into the agarose since they floated to the surface due to the air in the scaffolds.

Table A.2: Standard and long dehydration process for histological analysis optimization

Solution	**Standard**	**Long**
70% EtOH	60'	120'
80% EtOH	60'	120'
90% EtOH	60'	120'
100% EtOH	60'	120'
100% EtOH	60'	120'
Xylene	30'	60'
Xyelene	30'	60'
Paraffin	60'	120'

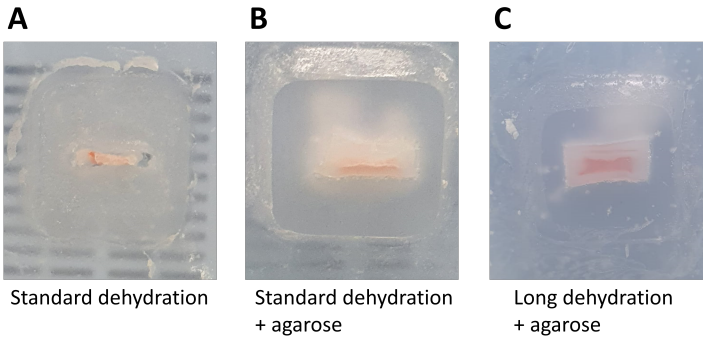

Figure A.9: Embedded scaffolds after three different dehydration procedures. A) Standard dehydration method. B) Standard dehydration method when scaffolds was embedded in agarose. C) Long dehydration method when scaffold were embedded in agarose.

A.7. Pellet study

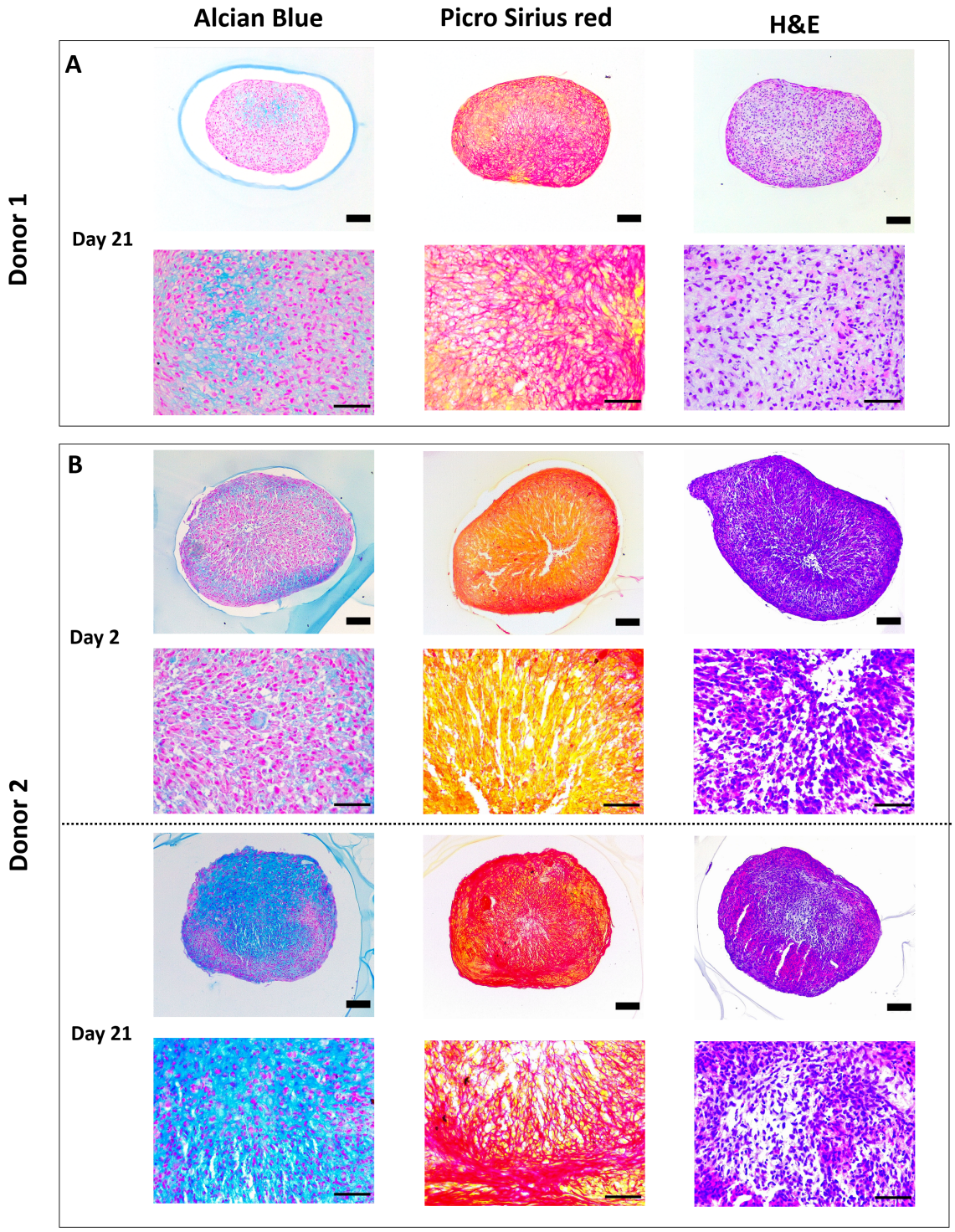

Figure A.10: Histological analysis of MSCs pellets with different donors cultured in chondrogenic differentiation medium for 21 days. The pellets were stained with Alcian Blue, Picrosirius Red and Hematoxylin & Eosin (H&E) and pictures were taken with 10x objective. Scale bar = 100 µm. A) Pellets of MSCs from donor 1 for day 21. B) Pellets of MSCs from donor 2 for day 2 and 21. These results were obtained by Maria Kalogeropoulou.

A.8. GAG analysis

The sulfated glycominoglycans (sGAG) production of the cells was analysed using the sulfated glycosaminoglycan assay (Blyscan). The sGAG assy kit used a cationic, blue dye, which binds to the negatively charged GAG's. However it does not stain HA, because HA is not sulfated. After bioprinting, the scaffolds were kept in culture for 28 days and every 2 days the medium was refreshed. Before refreshing, a small volume of the scaffold's culture medium of the past two days, was stored at -80°C for the sGAG analysis. For this assay, culture medium of $THA_{2.5}$, $THA_{2.5}$-$AC_{0.5}$ and $THA_{2.5}$-AC_1 scaffolds at day 1, 7 and 28 were tested.

The protocol of the sGAG analysis starts with combining 200 µL of medium with 1 mL of Blyscaon dye reagent. In addition, aliquots containing an increasing concentration of sGAG's (0 - 6 µg are used as reference standard to produce a calibration curve. For the reference standard the same procedure is used. Next, the samples are gently mixed for 30' under rotation (4 rpm). After mixing, the samples are centrifuged for 10' at 12000 rpm to create purple sGAG-dye pellets at the bottom of the tubes to avoid any pellets loss during the draining of the unbound dye. When the excessive dye is removed, 0.5 mL of dissociation reagent is added to the pellets. The samples are vortexed and subsequently mixed for 30' under rotation (4 rpm), so the pellet have been broken up and the bound dye has been dissolved. Next, 200 µL of each sample and the reference standard was transferred to a 96 micro well plate to measure the absorbance at a wavelength of 656 nm, using a microplate reader (PerkinElmer, Massachusetts, US).

The sGAG reference standard absorbance was plotted against its known concentrations. Joining the points resulted in a straight line that was extended downwards to near zero (Fig. A.11A). The concentration of the test sample could be calculated from the formula of the linear. The results of sGAG analysis of the bioprinted scaffolds are presented in Fig. A.11B. The sGAG production of the cells embedded in $THA_{2.5}$ and $THA_{2.5}$-AC_1 scaffolds showed no significant difference over time. For the $THA_{2.5}$-$AC_{0.5}$ scaffold an increase was observed for the sGAG producution of day 28 compared to day 1.

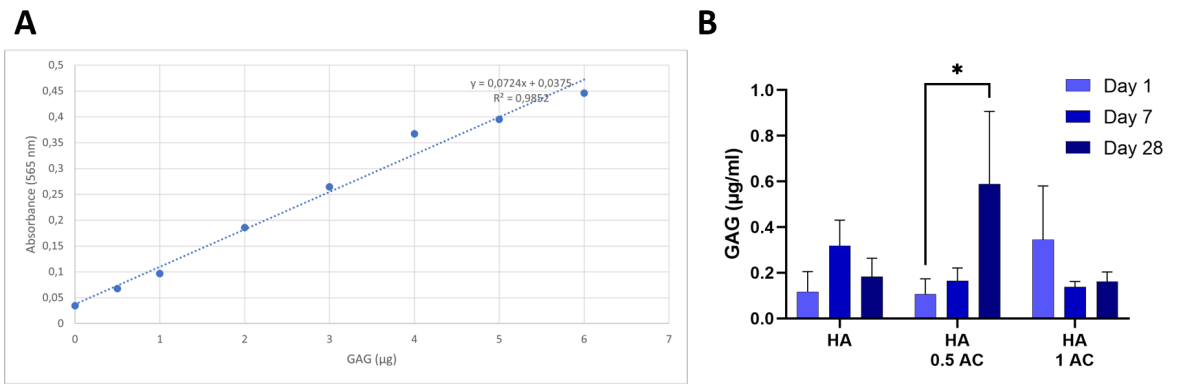

Figure A.11: GAG analysis of the scaffolds bioprinted with $THA_{2.5}$, $THA_{2.5}$-$AC_{0.5}$ and $THA_{2.5}$-AC_1 and cell density of 5 x 10^6 cells/ml. A) Calibration curve with y = 0.0724x + 0.0375 and R^2 = 0.9852 . B) The GAG production for day 1, 7 and 28.